PLOS GENETICS

RESEARCH ARTICLE

Two distinct lipid transporters together regulate invasive filamentous growth in the human fungal pathogen *Candida albicans*

Miguel A. Basante-Bedoya[1], Stéphanie Bogliolo[1], Rocio Garcia-Rodas[1,2], Oscar Zaragoza[2,3], Robert A. Arkowitz[1], Martine Bassilana[1]*

1 Université Côte d'Azur, CNRS, INSERM, iBV, Parc Valrose, Nice, FRANCE, **2** Mycology Reference Laboratory, National Centre for Microbiology, Health Institute Carlos III, Majadahonda, Madrid, Spain, **3** Center for Biomedical Research in Network in Infectious Diseases (CIBERINFEC-CB21/13/00105), Health Institute Carlos III, Madrid, Spain

* mbassila@unice.fr

Check for updates

OPEN ACCESS

Citation: Basante-Bedoya MA, Bogliolo S, Garcia-Rodas R, Zaragoza O, Arkowitz RA, Bassilana M (2022) Two distinct lipid transporters together regulate invasive filamentous growth in the human fungal pathogen *Candida albicans*. PLoS Genet 18(12): e1010549. https://doi.org/10.1371/journal.pgen.1010549

Editor: Aaron P. Mitchell, University of Georgia, UNITED STATES

Received: September 7, 2022

Accepted: November 29, 2022

Published: December 14, 2022

Copyright: © 2022 Basante-Bedoya et al. This is an open access article distributed under the terms of the Creative Commons Attribution License, which permits unrestricted use, distribution, and reproduction in any medium, provided the original author and source are credited.

Data Availability Statement: All relevant data are within the manuscript and its supporting information files.

Funding: This work was supported by the CNRS, INSERM, Université Côte d'Azur, and ANR (ANR-11-LABX-0028-01, ANR-16-CE13-0010-01 and ANR-19-CE13-0004-01) grants to RAA, MB, and grant SAF2017-86192 from the Spanish Ministry for Science and Innovation to RG, OZ. The funders had no role in study design, data collection and

Abstract

Flippases transport lipids across the membrane bilayer to generate and maintain asymmetry. The human fungal pathogen *Candida albicans* has 5 flippases, including Drs2, which is critical for filamentous growth and phosphatidylserine (PS) distribution. Furthermore, a *drs2* deletion mutant is hypersensitive to the antifungal drug fluconazole and copper ions. We show here that such a flippase mutant also has an altered distribution of phosphatidylinositol 4-phosphate [PI(4)P] and ergosterol. Analyses of additional lipid transporters, *i.e.* the flippases Dnf1-3, and all the oxysterol binding protein (Osh) family lipid transfer proteins, *i.e.* Osh2-4 and Osh7, indicate that they are not critical for filamentous growth. However, deletion of Osh4 alone, which exchanges PI(4)P for sterol, in a *drs2* mutant can bypass the requirement for this flippase in invasive filamentous growth. In addition, deletion of the lipid phosphatase Sac1, which dephosphorylates PI(4)P, in a *drs2* mutant results in a synthetic growth defect, suggesting that Drs2 and Sac1 function in parallel pathways. Together, our results indicate that a balance between the activities of two putative lipid transporters regulates invasive filamentous growth, *via* PI(4)P. In contrast, deletion of *OSH4* in *drs2* does not restore growth on fluconazole, nor on papuamide A, a toxin that binds PS in the outer leaflet of the plasma membrane, suggesting that Drs2 has additional role(s) in plasma membrane organization, independent of Osh4. As we show that *C. albicans* Drs2 localizes to different structures, including the Spitzenkörper, we investigated if a specific localization of Drs2 is critical for different functions, using a synthetic physical interaction approach to restrict/stabilize Drs2 at the Spitzenkörper. Our results suggest that the localization of Drs2 at the plasma membrane is critical for *C. albicans* growth on fluconazole and papuamide A, but not for invasive filamentous growth.

Author summary

Candida albicans is a human opportunistic fungal pathogen that diverged from *Saccharomyces cerevisiae* ~250 million years ago, in which a switch from budding growth to

analysis, decision to publish, or preparation of the manuscript.

Competing interests: The authors have declared that no competing interests exist.

filamentous hyphal growth is associated with virulence. We sought here to understand how membrane expansion in these hyperpolarized filamentous cells is regulated by lipid transport mechanisms, and in particular flippases that transport phospholipids across lipid bilayers, thus generating membrane lipid asymmetry. Deletion of one of these flippases results in cells defective for hyphal invasive growth, cell wall integrity and virulence, as well as increased sensitivity to the most commonly used antifungal drug fluconazole. We show that this flippase localizes to different cellular compartments and our results suggest that the plasma membrane localization is critical for growth on fluconazole, but not for invasive filamentous growth and cell wall integrity. Strikingly, our data reveal that a genetic interaction between homologs of two different lipid transporters, previously identified in *S. cerevisiae* budding growth, regulates *C. albicans* hyphal growth. An attractive possibility that merits investigation is whether this is a conserved feature of the fungal kingdom.

Introduction

Polarized growth is an essential process that is regulated, in particular, by cooperative interactions between key establishment proteins and specific lipids at the plasma membrane (PM). For instance in the baker's yeast *Saccharomyces cerevisiae*, dynamic nanoclusters of the Rho-GTPase Cdc42 are regulated by multivalent interactions between its sole activator Cdc24, the scaffold protein Bem1 and anionic lipids, including PS [1–3]. Similarly, in the fission yeast *Schizosaccharomyces pombe*, the localization and function of the two essential Rho-GTPases, Cdc42 and Rho1, depend on polarized PS distribution [4]. The importance of anionic lipids, and PS in particular, for cellular function and signaling encompasses kingdoms from fungi, to mammals [5] to plants [6]. In addition, PS has been reported to be critical for virulence in a broad spectrum of microbial pathogens (reviewed in [7,8]). In particular, in the human fungal pathogen *Candida albicans*, the PS synthase Cho1, which is conserved in fungi but does not have an ortholog in Humans, is required for virulence in a murine candidiasis model [9]. A *cho1* deletion mutant also exhibits increased exposure of β(1,3)-glucan *via* up-regulation of cell wall MAPK cascades, facilitating its detection by innate immune cells [10]. PS is synthesized in the endoplasmic reticulum (ER) and its cellular distribution is regulated both by lipid transfer proteins (LTPs), which function at contact sites between the ER and the target cellular compartments, and lipid transporters, such as flippases that establish PS asymmetry between membrane leaflets (reviewed in [11]).

Lipid flippases are P4-ATPases, only found in eukaryotes, where they are similar in domain structures from fungi to Humans (reviewed in [12]). These proteins actively transport phospholipids from the external/luminal to cytoplasmic membrane leaflets and play an important role in polarized growth (reviewed in [13]). There are 14 P4-ATPases in Humans and only 5 in the yeast *S. cerevisiae* (Dnf1-3, Drs2, Neo1), with most of them regulated by non-catalytic subunits from the Cdc50/Lem3 family. For example, in *S. cerevisiae*, Cdc50 forms a functional complex with Drs2 [14,15] and very recently, the cryo-electron microscopy structure of different conformations of this complex was resolved at 2.8 to 3.7 Å [16]. This complex, which is well characterized, both *in vitro* and *in vivo*, primarily transports PS [17,18]. The role of lipid flippases on membrane curvature and in trafficking has been extensively studied in *S. cerevisiae*, as well as in mammals (reviewed in [19]). In *S. cerevisiae*, Neo1, which is the sole essential flippase [20], localizes to the Golgi and endomembranes, Drs2 and Dnf3 to the trans-Golgi network (TGN) and Dnf1-2 to the PM [17,21,22]. A recent study indicates that Dnf3 can also

be found at the PM in a cell-cyle dependent fashion, where it regulates, together with Dnf1-2, *S. cerevisiae* pseudohyphal growth [23]. Furthermore, in response to pheromone, it was shown that Dnf1, Dnf2 and Dnf3 localize to the schmoo tip, while Drs2 remains at the Golgi [24]. Interestingly, in the filamentous fungi *Aspergillus nidulans* and *Fusarium graminearum*, it was shown that the Drs2 homolog, DnfB, localizes primarily to a cluster of vesicles at the hyphal apex, called the Spitzenkörper (SPK), which is characteristic of fungi that grow in a filamentous form [25,26]. Together, these data indicate that flippases can localize to different compartments in specific conditions of polarized growth.

LTPs and more specifically oxysterol-binding protein (OSBP)-related proteins (ORPs), are also important for membrane lipid composition, *via* non-vesicular traffic (reviewed in [27]), including for PS distribution (reviewed in [11]). LTPs can bind specific ligands such as PI(4)P, PS and sterol. For example, in *S. cerevisiae*, there are 7 oxysterol-binding homology (Osh) proteins, among which Osh6/Osh7 transports PS from cortical ER (cER) and PM [28], in counter-exchange with PI(4)P [29]. On the other hand, another Osh protein, Kes1, which is homolog to Osh4 and transports sterol in counter-exchange with PI(4)P [30], was proposed to act antagonistically with Drs2 to regulate the sterol distribution between PM and internal membranes in *S. cerevisiae* [31].

Filamentous fungi are highly polarized organisms, in which the role of flippases has been investigated. In *A. nidulans*, the homologs of Dnf1 and Drs2, *i.e.* DnfA and DnfB, regulate growth and PS asymmetry [25], while in *Magnaporthe grisea*, Mg*APT2*, one of the 4 amino-phospholipid translocase (APT) encoding genes related to Drs2, is required for plant infection but not filamentous growth [32]. In *F. graminearum*, flippases play redundant as well as distinct roles in vegetative growth, where FgDnfA is critical, stress response, reproduction and virulence [26,33,34]. In the human fungal pathogen *C. albicans*, deletion of either Dnf1 or Dnf2 results in moderate increase sensitivity to copper [35]. The *drs2* deletion mutant is hypersensitive to copper [35], as well as to the antifungal drug fluconazole [36]. Deletion of Drs2 also results in altered PS distribution and impaired filamentous growth [36], and that of its Cdc50 subunit in altered filamentous growth and reduced virulence in a murine candidiasis model [37]. Here, we sought to determine more specifically the role of Drs2 in morphogenesis and whether PS asymmetry is critical for this process.

Our results show that in response to serum, of the four flippases Dnf1-3 and Drs2, only Drs2 is critical for filamentous growth, with Dnf2 having a minor role in this process. Filamentous growth was largely restored in the *drs2* mutant upon deletion of the LTP Osh4, but not by that of other Osh proteins (Osh2, Osh3 and Osh7). Furthermore, our results demonstrate that the distribution of PS and of the phosphatidylinositol phosphate PI(4)P, which are both altered in the *drs2* mutant, is restored upon deletion of *OSH4*. These data indicate that the requirement for flippase activity across the lipid bilayer during filamentous growth can be specifically bypassed by lipid exchange between membrane compartments.

Results

Drs2 has a unique role in *C. albicans*

In *A. nidulans*, the Drs2 homolog DnfB, is not critical for hyphal growth [25]. In contrast, in *C. albicans*, Drs2 is required for filamentous growth, whereas budding growth is largely unaffected (mean doubling time of 90 min, compared to 80 min in the wild-type strain) [36]. We investigated the importance of other flippases, *i.e.* Dnf1, Dnf2 and Dnf3, using loss of function mutants that we generated (S1A Fig). As illustrated in Fig 1A, a *drs2* deletion mutant was not invasive on serum-containing media. In contrast, deletion of *DNF1* or *DNF3* did not alter serum-induced invasive growth, while deletion of *DNF2* resulted in reduced invasive growth,

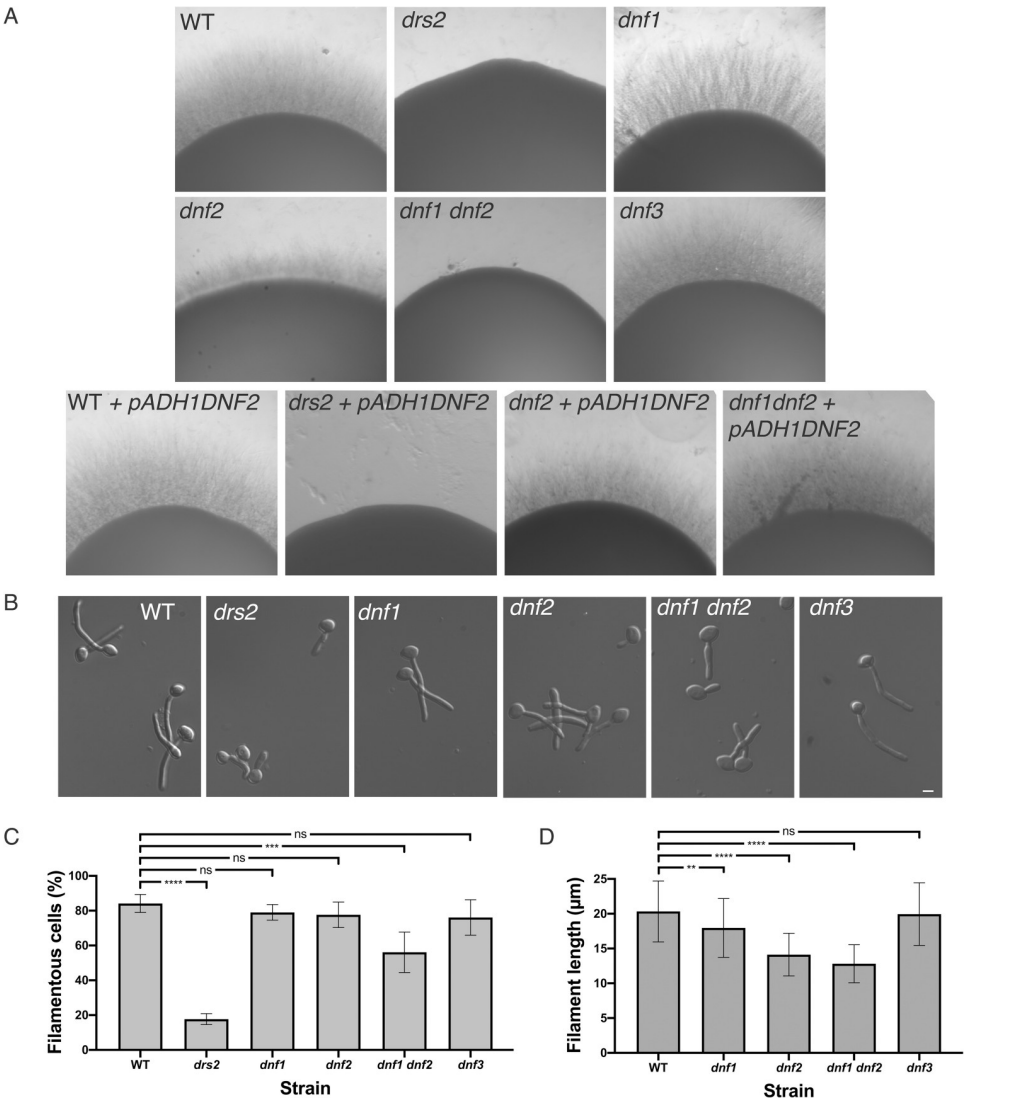

Fig 1. Drs2 is critical for hyphal invasive growth. A) Invasive filamentous growth cannot be restored by overexpression of *DNF2* in the *drs2/drs2* mutant. The indicated strains, WT (PY4861), *drs2/drs2* (*drs2*, PY3375), *dnf1/dnf1* (*dnf1*, PY6235), *dnf2/dnf2* (*dnf2*, PY5814), *dnf3/dnf3* (*dnf3*, PY5801), *dnf1/dnf1 dnf2/dnf2* (*dnf1 dnf2*, PY6400), WT + *pADH1DNF2* (PY5005), *drs2/drs2* + *pADH1DNF2* (*drs2* + *pADH1DNF2*, PY5003), *dnf2/dnf2* + *pADH1DNF2* (*dnf2* + *pADH1DNF2*, PY5919), and *dnf1/dnf1 dnf2/dnf2* + *pADH1DNF2* (*dnf1 dnf2* + *pADH1DNF2*, PY5922), were grown on agar-containing YEPD with serum and images were taken after 6 days. Similar results were observed in 2 independent experiments. B) *DRS2* is specifically required for hyphal growth in response to serum. Cells from the indicated strains were incubated with serum for 90 min at 37˚C. Bars are 5 μm. C) and D). Graphs represent the percentage of hyphae (C) and the filament length (D) in the indicated strains grown as in 1B. The percentage of hyphae was 84 ± 5%, 79 ± 4%, 78 ± 7%, 76 ± 10%, 56 ± 12% and 18 ± 3% for wild-type and the *dnf1*, *dnf2*, *dnf3*, *dnf1 dnf2* and *drs2* deletion mutants, respectively (average of 3 experiments with $n \sim 150$ cells each). The filament length was measured from the junction between cell body and filament (error bars indicate the mean +/- the SD of 3 experiments, $n \sim 50$ cells each). **, $P < 0.01$; ***, $P < 0.0005$; **** $P < 0.0001$; ns, not significant.

https://doi.org/10.1371/journal.pgen.1010549.g001

which was further reduced in a double *dnf1dnf2* deletion mutant. Over-expression of *DNF2* restored invasive growth in the *dnf2* and *dnf1 dnf2* mutants, but not in the *drs2* mutant, suggesting that Dnf2 and Drs2 do not functionally overlap in this invasive growth process. Upon serum-induced hyphal growth in liquid media (Fig 1B–1D), the *dnf1*, *dnf2* and *dnf3* deletion mutants produced hyphae similar to the wild-type cells, with hyphal formation in the *dnf1*

dnf2 cells somewhat reduced. The average hyphal filament length at 90 min was, nonetheless, slightly reduced in *dnf2* cells as well as in *dnf1 dnf2* (14 ± 3 μm and 13 ± 3 μm, respectively) compared to the WT, *dnf1* and *dnf3* cells (20 ± 4 μm, 18 ± 4 μm and 20 ± 4 μm, respectively). These results are in agreement with very recent data, which also show that both a *dnf2* and a *dnf1 dnf2* mutant exhibit reduced invasive filamentous growth in response to the nutrient poor spider media, another inducer of filamentous growth [38]. These data indicate that, in contrast to the *drs2* deletion mutant, *dnf1*, *dnf2* and *dnf3* deletion mutants undergo filamentous growth similar to the wild-type cells, albeit with a reduced efficiency for *dnf2*. Furthermore, Fig 2A and 2B shows that the *dnf1-3* mutants also grew similar to the wild-type cells in the presence of the cell wall perturbants calcofluor white (CFW) and congo red (CR), the antifungal drugs, caspofungin (Caspo) and fluconazole (FCZ), and the detergent sodium dodecyl sulfate (SDS), with only the *dnf2* mutant growth somewhat reduced on 0.05% SDS. In contrast, the *drs2* mutant was hypersensitive to SDS, in addition to CFW and FCZ [36]. The growth defect of *drs2* cells on FCZ could result from a mislocalization of multi-drug transporters, such as Cdr1 [39]. Fig 2C shows that, although a Cdr1-GFP fusion protein was detected at the PM in *drs2* cells, 79 ± 8% of the cells had internal Cdr1 signal, in contrast to wild-type and complemented cells, suggesting that PM targeting of MDR is partially impaired in *drs2* cells. Together, these data indicate that Drs2 has a unique role in *C. albicans*.

Drs2 is critical for hyphal extension after septin ring formation

In response to serum, *drs2* cells appear to initiate filamentous growth, although they were unable to form hyphae [36] and invasive colonies (Fig 1A), and reintroduction of a copy of *DRS2* in this mutant restored invasive growth (Fig 3A). We examined this mutant in a murine model for systemic candidiasis and Fig 3B shows that the *drs2* mutant causes no lethality, compared to the wild-type and complemented strains, at 16 days post injection. At the transcriptional level, hyphal growth is controlled by the hyphal specific cyclin *HGC1*, which is further regulated by the transcription factor *UME6* [40]. Both *hgc1* and *ume6* deletion mutants are defective in hyphal extension and attenuated for virulence in a mouse infection model [41,42]. Quantitative RT-PCR analyses in Fig 3C show that, upon serum exposure, *HGC1* and *UME6* were up-regulated in the *drs2* mutant compared to budding cells (>100-fold for *HGC1* and 40-fold for *UME6*), with a level of induction of *HGC1* slightly reduced compared to that of the wild-type cells. Similarly, *ECE1*, which encodes the peptide toxin candidalysin and whose expression correlates with cell elongation [43], *HWP1*, which encodes a hyphal cell wall protein associated with hyphal development [44] and *ALS3*, which encodes an agglutinin-like (Als) adhesin [45], were all up-regulated in the *drs2* mutant upon serum exposure, with levels slightly reduced (3- to 5-fold) compared to the control cells. Only the induction of *SAP6*, which encodes a secreted acid protease [46], was substantially reduced (~ 10-fold) in *drs2*. Together, these data indicate that the *drs2* mutant hyphal growth defect is unlikely due to the modest reduction of *HGC1* induction.

To further characterize the *drs2* mutant at the molecular level, we used time-lapse microscopy to follow cells expressing fluorescent reporters for different cellular compartments. Fig 4A illustrates representative time courses of hyphal growth both in WT and *drs2* cells expressing a fluorescently tagged septin Cdc10 [47]. Measurements of the diameters of filament compartments, apical (pre-septum) and distal (post-septum) to the septin ring (Fig 4B), show that, while it remained constant in wild-type cells (1.8 ± 0.2 μm), the diameter increased in the apical compartments of *drs2* cells by about 40% (to 2.5 ± 0.3 μm). This increase was associated with a reduced extension rate (on average 0.09 μm/min in *drs2* cells, compared to 0.34 μm/min in WT cells; Fig 4C). These data are consistent with a defect in polarized growth in the

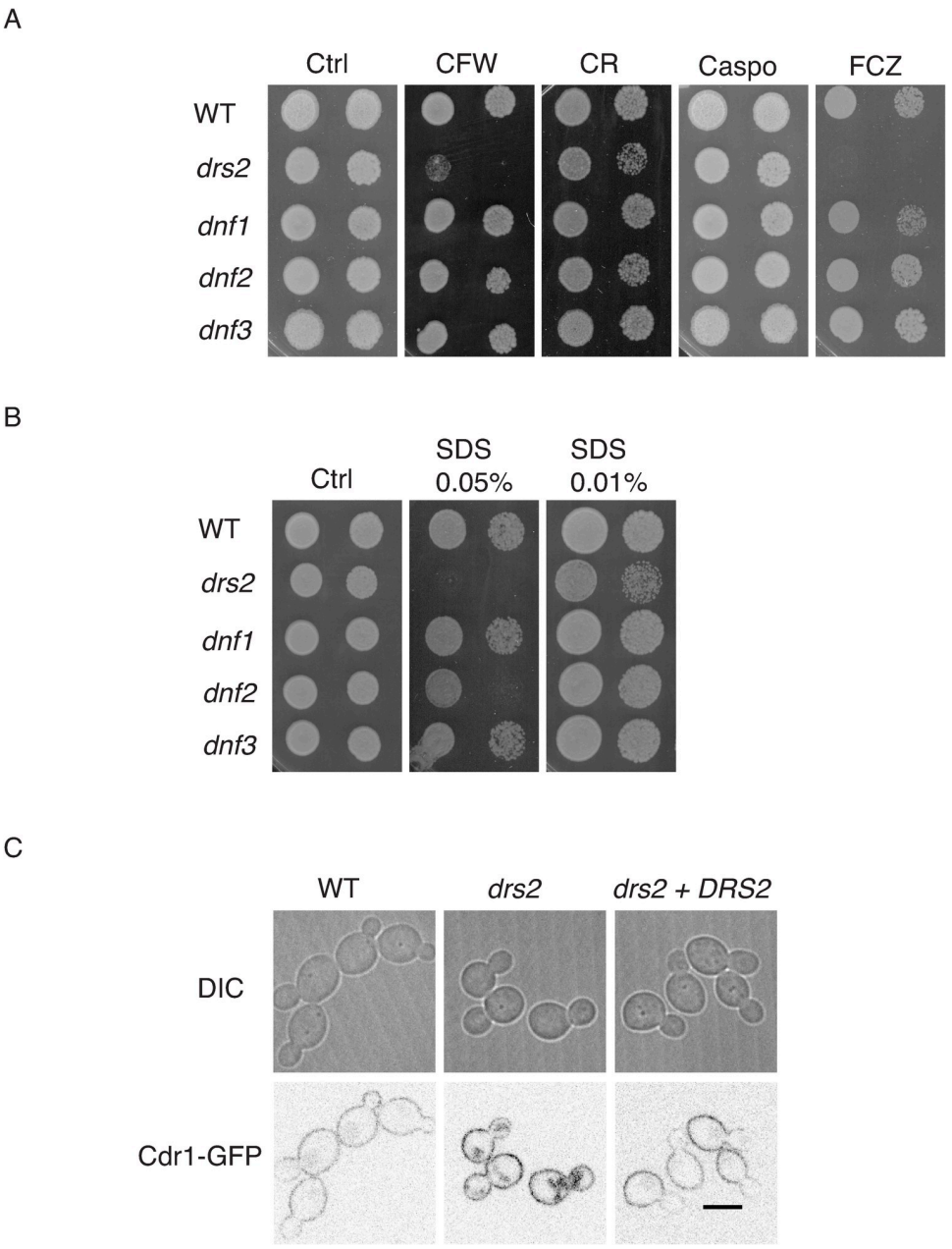

Fig 2. Drs2 has a unique role in *C. albicans*. (A). The *drs2* mutant has specific increased susceptibility to fluconazole and calcofluor white. Serial dilutions of indicated strains, as in Fig 1, were spotted on YEPD media (Ctrl) containing 25 μg/ml calcofluor white (CFW), 400 μg/ml Congo red (CR), 125 ng/ml caspofungin (Caspo) or 5 μg/ml fluconazole (FCZ). Images were taken after 2 days at 30˚C. Similar results were observed in 2 independent experiments. (B). The *drs2* mutant has increased susceptibility to SDS. Serial dilutions of indicated strains, grown as in 2A, were spotted on YEPD media (Ctrl) containing 0.01% or 0.05% SDS. (C). PM targeting of the multidrug ABC transporter Cdr1 is altered in *drs2* cells. Central z-sections of representative wild-type (WT, PY6393), *drs2*/*drs2* (*drs2*, PY6395) and *drs2*/*drs2* + *pDRS2DRS2* (*drs2* + *DRS2*, PY6646) cells expressing Cdr1-GFP are shown.

https://doi.org/10.1371/journal.pgen.1010549.g002

drs2 mutant after the first septin ring forms. In agreement with this, we observed that, upon filament extension, active Cdc42, visualized with the CRIB (Cdc42 Rac1 Interactive Binding domain) reporter [48], became depolarized in *drs2* cells and the SPK (visualized with the myosin light chain Mlc1, [49,50]), was not maintained at the filament tip following cell division,

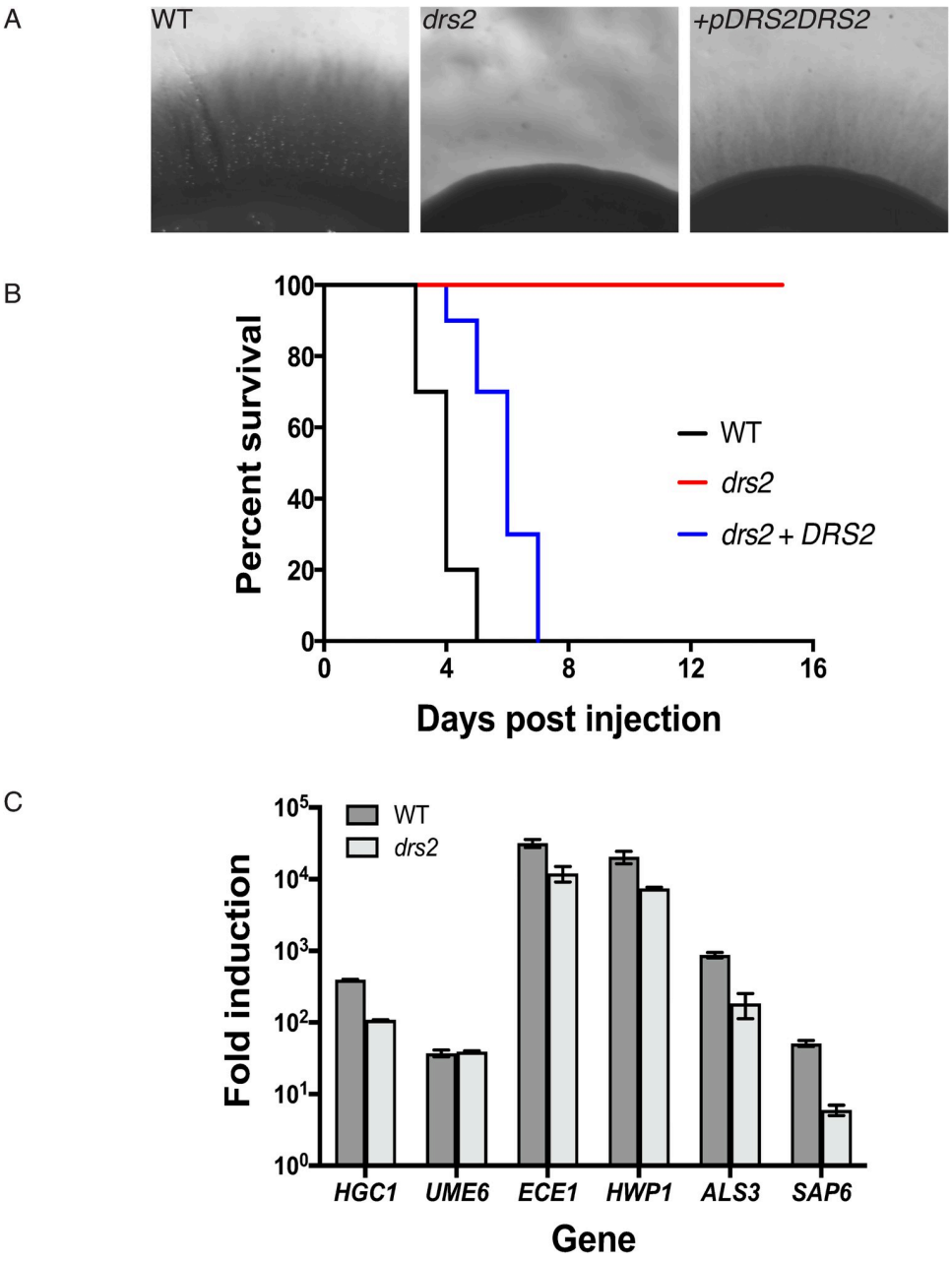

Fig 3. Drs2 is critical for virulence in a mouse model of systemic candidiasis. A) Reintroduction of *DRS2* complements the invasive growth defect of the *drs2* mutant. The indicated strains WT (PY4861), *drs2/drs2* (*drs2*, PY3375), and *drs2/drs2* + *pDRS2DRS2* (*drs2* + *DRS2*, PY5042), were grown as in Fig 1A and 1B) The *drs2* mutant has attenuated virulence in a mouse model of hematogenously disseminated candidiasis. Balb/C mice (n = 10) were injected with an inoculum (5 x 10^5 cells) of the indicated strains and the survival was assessed. C) Hyphal specific gene are induced in *drs2* cells upon serum exposure. mRNA and cDNA were prepared from the indicated strains grown 120 min in the presence of serum. *HGC1*, *ECE1*, *HWP1*, *ALS3* and *SAP6* transcripts were determined by qRT-PCR using primer pairs described in [89], and *UME6* transcripts were determined using UME6.pTm/UME6.mTm (89 bp) primer pair. Bars indicate the mean ± SD (n = 3 determinations). Similar results were observed in an additional biological replicate. NAD-linked Glyceraldehyde-3-phosphate dehydrogenase (*TDH3*) transcript levels were used for normalization.

https://doi.org/10.1371/journal.pgen.1010549.g003

compared to the control cells (Fig 4D–4E). Furthermore, comparison of the wild-type and *drs2* cells expressing both reporters for active Cdc42 and the Spitzenkörper, indicates that depolarization of Cdc42 occurred prior to the SPK delocalization from the filament tip (S1 and S2 Movies). Together, these data indicate that, subsequent to septin ring formation, the *drs2* mutant is unable to redirect or reinitiate growth to the apex, which ultimately results in growth arrest and/or pseudohyphal growth.

Drs2 localizes to the hyphal tip

In *S. cerevisiae*, Drs2 localizes to the late Golgi during budding [20] and mating [24], while its homolog in *A. nidulans*, DnfB, localizes within the SPK core [25]. To examine the distribution of Drs2 in *C. albicans*, we generated a strain that expresses a functional *DRS2-GFP* fusion (Fig 5A). Given that the homolog of Dnf1-2 in *A. nidulans*, DnfA, also localizes to the Spitzenkörper, albeit to the outer layer macrovesicles compared to DnfB [25], we also generated a strain that expressed a functional *DNF2-GFP* fusion (Fig 5A). Fig 5B shows that Drs2 was restricted to the apical region of the hyphal tip, as well as in internal structures, likely Golgi cisternae by analogy with *S. cerevisiae* [20]. Dnf2 was essentially localized at the tip crescent, similar to its localization in *S. cerevisiae* at bud tips and mating projections [24]. Both Dnf2 and Drs2 co-localized with a PM marker (a prenylated RFP fusion, RFP-CtRac1, [51]), although Drs2 localized to a more restricted region of the hyphal tip than Dnf2 (Fig 5C). Drs2 also partially co-localized with the SPK marker, Mlc1 (Fig 5D), which could be due to the proximity (less than 100 nm) of this structure to the PM [52]. These data indicate that Drs2 and Dnf2 have distinct distributions at the filament apex.

The *drs2* mutant is altered for PI(4)P distribution

Drs2 is a P4-ATPase that flips PS selectively across the lipid bilayer *in vitro* and *in vivo* in *S. cerevisiae* [17,18]. In *C. albicans*, using the reporter Lactadherin C2 (LactC2) [53–55], we observed that the distribution of PS was altered during hyphal growth in the *drs2* mutant, as the reporter was visible in an intracellular punctate pattern [36]. To determine the impact of the *DRS2* deletion on the distribution of other lipids, shown to be critical for hyphal growth, such as the phosphatidylinositol phosphates PI(4)P and PI(4,5)P_2 [56,57], as well as ergosterol [58], we used specific fluorescent reporters. The distribution of PI(4,5)P_2 appears to be similar in wild-type cells and *drs2* filamentous cells (Fig 6A), yet the distribution of PI(4)P was substantially less polarized in the mutant, compared to the wild-type or complemented strains (Fig 6B). This depolarization is further illustrated by the graph in Fig 6B, which shows the relative concentration of PI(4)P, as a function of filament length. In contrast, PI(4)P at the Golgi was largely unaffected in *drs2*, compared to WT cells, both during filamentous growth (Fig 6C), and budding growth (mean of 7.1 ± 2.8 Golgi cisternae per cell in *drs2* cells compared to 7.8 ± 2.4 in the wild-type control, Fig 6D). These data indicate that deletion of *DRS2* results in altered distribution of PM PI(4)P, but not PI(4,5)P_2.

Using filipin staining, it was shown that membrane sterols are highly concentrated at the apex during *C. albicans* hyphal growth, with such a polarization not observed in budding and pseudohyphal cells [58]. We examined sterol distribution, using both filipin staining and the genetically encoded biosensor D4H. This biosensor consists of the Domain 4 of perfringolysin O, a toxin produced by *Clostridium perfringens*, used to monitor sterols *in vivo* [59–62]. Fig 7A shows that sterols are highly concentrated at the apex of WT hyphal cells, irrespective of the reporter used. In contrast, in the *drs2* mutant, the D4H reporter preferentially labeled internal structures and reintroduction of a copy of *DRS2* restored the ergosterol distribution to the PM

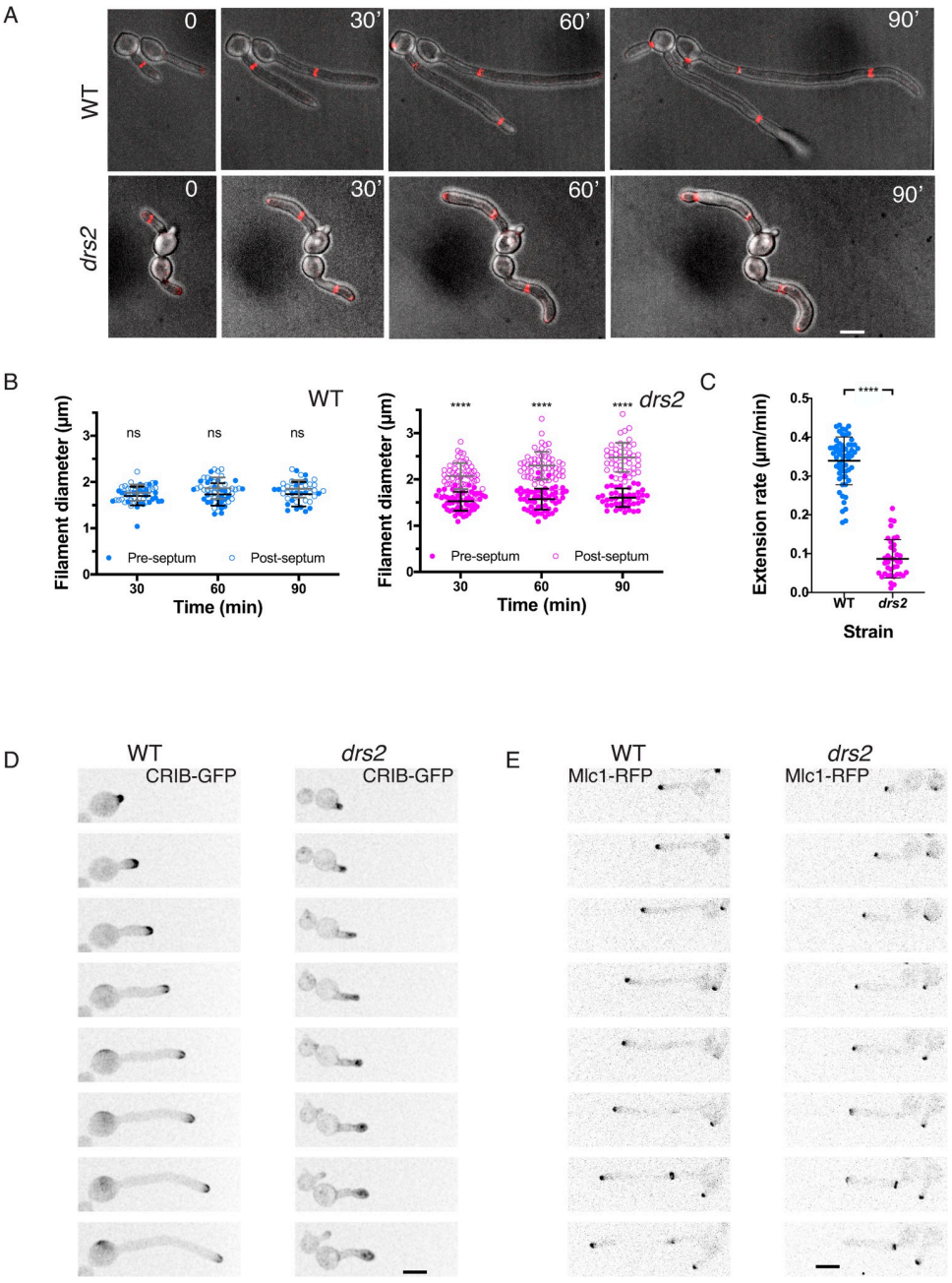

Fig 4. Drs2 is critical for maintaining polarized filament extension. A) Both cell morphology and filament extension rate are altered in the *drs2* mutant, after septin ring formation. Time lapse of wild-type (WT, PY5613) and *drs2*/*drs2* (*drs2*, PY5615) cells expressing Cdc10-mScarlet, incubated in the presence of serum. Images were taken every 10 min and merges between DIC and sum projections of 21 z-sections are shown. Bars are 5 μm. B) Graphs represent the filament diameter before (open circles) and after (solid circles) the first septin ring, as a function of the times from the first image in which the septin ring is observed in wild-type (blue) and *drs2* (magenta) cells. Means ± SD of 25–50 cells are shown. **** $P < 0.0001$; ns, not significant. C) The graph shows the filament extension rate in wild-type (blue) and *drs2* (magenta) cells. Means ± SD of 30–60 cells are shown. D) and E) Polarized growth is altered in the *drs2* mutant. D) Time lapse of wild-type (WT, PY2263) and *drs2* cells (*drs2*, PY4972) expressing CRIB-GFP, incubated in the presence of serum. Images were taken every 10 min and maximum projections of 21 z-sections are shown. E) Time lapse of wild-type (WT, PY5349) and *drs2*/*drs2* cells (*drs2*, PY5218) expressing Mlc1-mScarlet, incubated in the presence of serum. Images were taken every 5 min and sum projections of 23 z-sections are shown.

https://doi.org/10.1371/journal.pgen.1010549.g004

(Fig 7B). Together, these data indicate that deletion of *DRS2* results not only in altered distribution of PM PS, but also of PI(4)P and ergosterol.

Deletion of *OSH4* in the *drs2* mutant restores invasive filamentous growth and plasma membrane PI(4)P distribution

LTPs can bind specific ligands such as PI(4)P, PS and sterol and, in *S. cerevisiae*, it was shown that Osh6/Osh7 transports PS in counter-exchange with PI(4)P [29], while Kes1 transports sterol in counter-exchange with PI(4)P [30]. *C. albicans* has 4 Osh proteins (Osh2-4 and Osh7), with Osh4 and Osh7 sharing ~ 60% identity with their *S. cerevisiae* counterparts, however their function is unknown in this organism. Note that the genes encoding *OSH7* (called *OBPA* and *OBPALPHA*) are located at the mating-type-like locus (MTL), similar to those encoding the Golgi phosphatidylinositol kinase Pik1 (*PIKA* and *PIKALPHA*).

To investigate the importance of Osh proteins in *C. albicans* invasive hyphal growth, we first generated *osh4* and *osh7* deletion mutants, as well as *drs2 osh4 and drs2 osh7* double deletion mutants (S1B Fig), and examined these mutants for invasive hyphal growth in response to serum. While deletion of *OSH4* or *OSH7* alone did not alter invasive growth, deletion of *OSH4*, but not *OSH7*, in the *drs2* mutant restored invasive growth to a level similar to that of WT cells (Fig 8A). In serum-containing liquid media, we also observed a rescue of hyphal growth upon deletion of *OSH4* in the *drs2* mutant (Fig 8B). In this *drs2 osh4* mutant, hyphal length was only slightly reduced compared to that of the wild-type and *osh4* cells (17 ± 3 μm, compared to 19 ± 1 μm for WT and *osh4* cells). To confirm the specificity of the *OSH4* deletion in restoring invasive growth in the *drs2* mutant, we also generated *drs2 osh2* and *drs2 osh3* double deletion mutants (S2A Fig). *Candida albicans OSH3* has been reported to be important for invasive growth in nutrient poor media (Spider media), but not in the presence of serum [63]. Similarly, we observed that mutants deleted for either *OSH2* or *OSH3* alone exhibited invasive growth in the presence of serum (S2B Fig). In contrast to *OSH4* deletion, absence of either *OSH2* or *OSH3* did not rescue the *drs2* invasive growth defect, although colonies from the *drs2 osh3* mutant were somewhat crenelated compared to the control strains (S2B Fig). Furthermore, while the *osh2* and *osh3* mutants formed hyphae similar to those of the wild-type (83 ± 5%, 73 ± 9% and 86 ± 6% for the WT, *osh2* and *osh3* strains, respectively), the percent of hyphae in the *drs2 osh2* and *drs2 osh3* mutants was similar to that of *drs2* (8 ± 6% and 21 ± 7%, respectively, compared to 19 ± 8% in *drs2*) (S2C Fig). These data indicate that, while Osh proteins (Osh2-4 and Osh7) are not required *per se* for serum-induced invasive filamentous growth, deletion of O*SH4* specifically bypasses the *drs2* requirement in this process. Notably, *OSH4* expression was not significantly altered in *drs2* cells, compared to the WT cells (S1C Fig).

To better characterize the mechanisms underlying the rescue of hyphal growth in the *drs2 osh4* mutant, we examined whether deletion of *OSH4* also restored the lipid distribution in the *drs2* mutant. Fig 9A shows that the distribution of PI(4)P was polarized in the *drs2 osh4* double mutant, similar to that in wild-type and *osh4* cells. Similarly, deletion of *OSH4* in the *drs2* mutant significantly restored PS distribution, as internal punctae were absent in *drs2 osh4* cells, similar to the wild-type, complemented and *osh4* strains (Fig 9B). Quantification of the LactC2 signal in the *drs2* mutant shows that the fraction of PS was reduced at the PM and increased internally, compared to wild-type and *osh4* cells, resulting in a decreased ratio of PM to intracellular signals (Fig 9B). Deletion of *OSH4* in *drs2* significantly increased this ratio, with an increase in PM signal, as well as a decrease in internal signal (Fig 9B). In contrast, the overall distribution of ergosterol appears similar in *drs2* and *drs2 osh4*, with the presence of a number of internal punctae, compared to wild-type and *osh4* cells (Fig 9C). The ergosterol tip

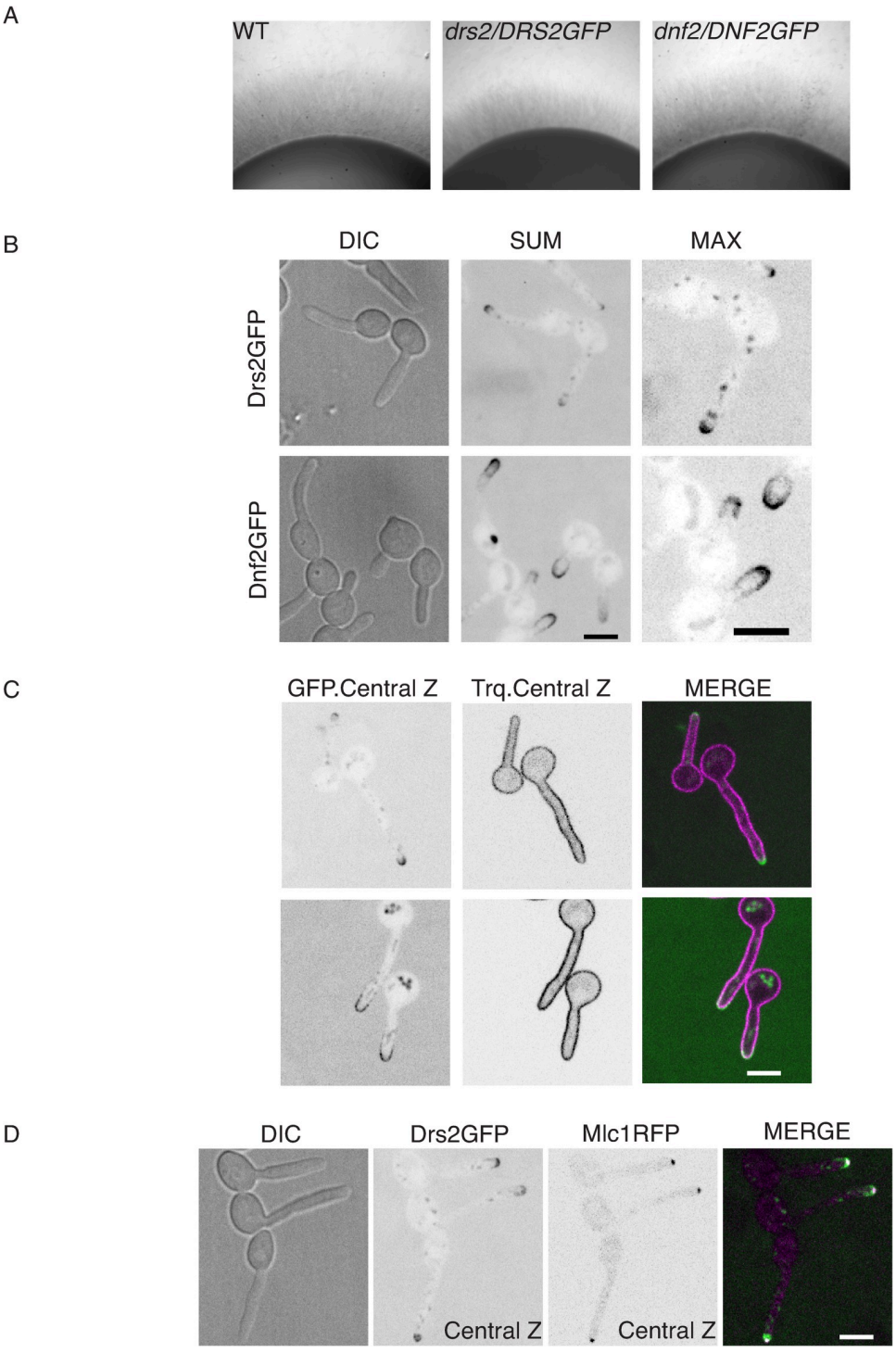

Fig 5. Drs2 localizes preferentially to the filament apex. A) The Drs2-GFP and Dnf2-GFP fusions are functional. The indicated strains, WT (PY4861), *drs2/DRS2GFP* (PY4665) and *dnf2/DNF2GFP* (PY5746) were grown as in Fig 1A and 1B) and C) Drs2 and Dnf2 localize differently to the filament apex. Sum projections and zoom images of Max projections of 16 z-sections of representative cells expressing Drs2-GFP and Dnf2-GFP after 90 min serum induction are shown (B). Central z-sections and merge of representative cells expressing mScarlet-CtRac1, together with either Drs2-GFP (PY6241) or Dnf2-GFP (PY6239), after 90 min serum induction are shown (C). D) Drs2 partially overlaps with Mlc1. Central z-section and merge of representative cells expressing Drs2-GFP together with Mlc1-mScarlet (PY4928), after 90 min serum induction are shown. Bars are 5 μm.

https://doi.org/10.1371/journal.pgen.1010549.g005

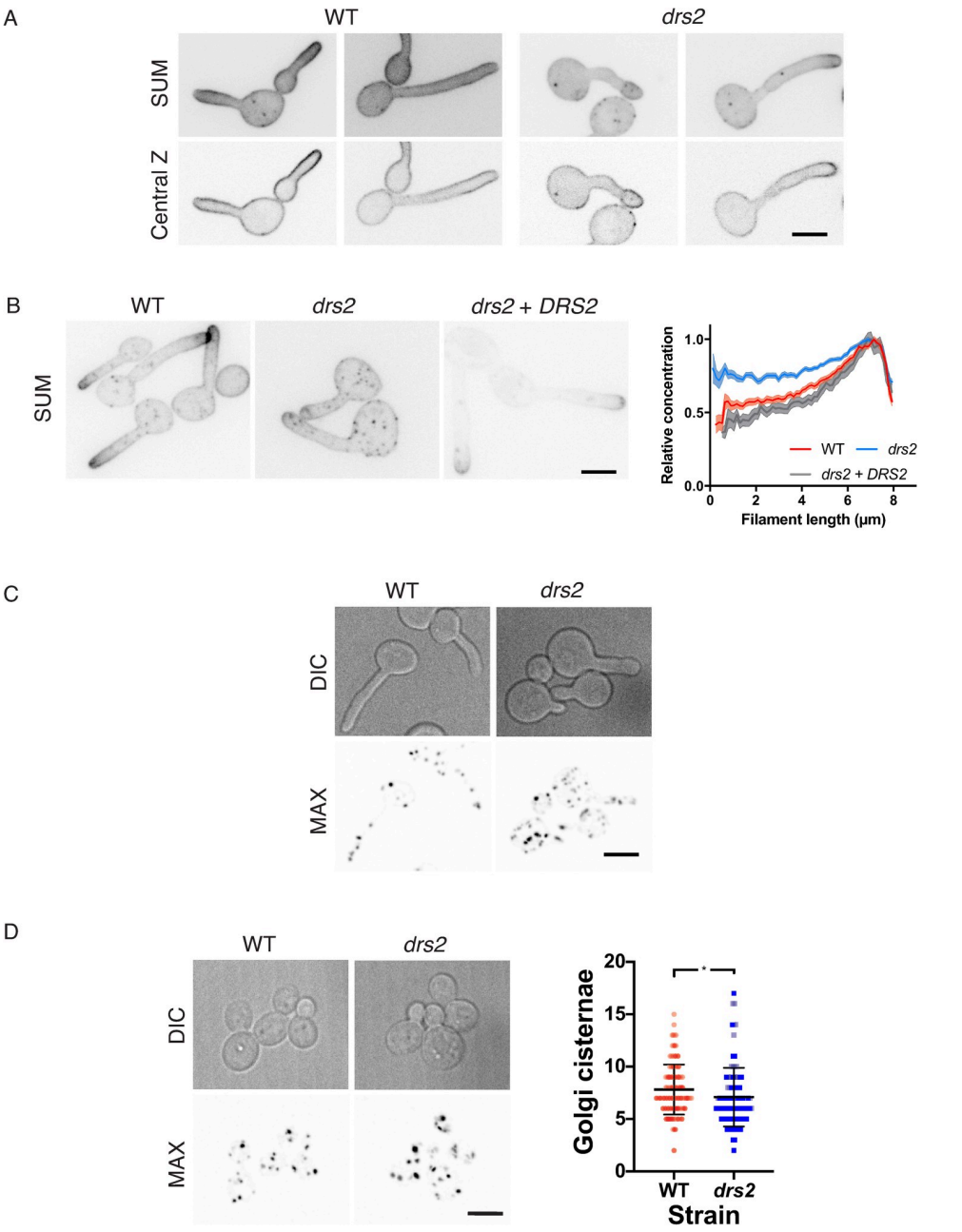

Fig 6. Plasma membrane PI(4)P distribution is altered in the *drs2* mutant. A) PM PI(4,5)P_2 distribution is not altered in the *drs2* mutant. Wild-type (PY1206) and *drs2/drs2* cells (*drs2*, PY4050) expressing GFP-$(PH^{PLC\delta1})_2$-GFP were incubated for 60 or 90 min, respectively, in the presence of serum. Sum projections (21 z-sections) and central z-sections of representative cells are shown. B) PM PI(4)P distribution is altered in the *drs2* mutant. The indicated cells, WT (PY5619), *drs2/drs2* (*drs2*, PY5568) and *drs2/drs2* + *pDRS2DRS2* (*drs2* + *DRS2*, PY6407) expressing GFP-$(PH^{OSH2\ [H340R]})_2$-GFP were incubated for 90 min in the presence of FCS. Sum projections of (21 z-sections) of representative cells are shown. The graph illustrates the means ± the SEM of the relative concentration of PM PI(4)P as a function of filament length, normalized to the maximal signal for each cell (n = 25–60 cells). C) and D) The number of Golgi cisternae is not substantially affected in the *drs2* mutant. DIC and maximum projections (21 deconvolved z-sections) of representative WT (PY2578) and *drs2/drs2* cells (*drs2*, PY3873) expressing $FAPP1^{[E50A,H54A]}$-GFP incubated in the presence of serum are shown (C). The number of Golgi cisternae per cell was determined in budding cells of the indicated strains from maximum projections of deconvolved images (21 z-sections). (D). Bars indicate the mean ± the SD of 3 independent biological samples (n = 100 cells and ~700–800 cisternae for each strain). * $P < 0.05$.

https://doi.org/10.1371/journal.pgen.1010549.g006

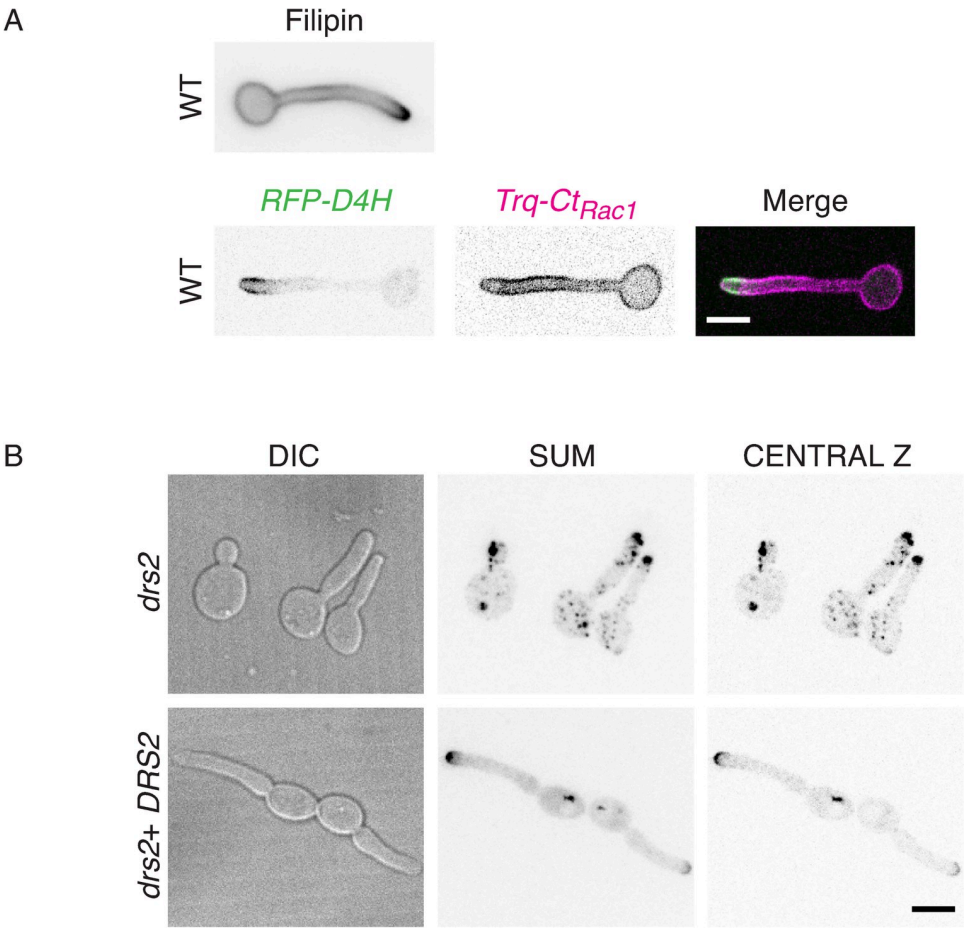

Fig 7. Distribution of ergosterol is altered in the *drs2* mutant. A) The ergosterol reporters Filipin and D4H localize similarly at the apex of the filament in wild-type cells. Top panel: Wild-type cells (PY4861) were induced serum prior to staining with filipin, as described [58]. Images were taken with a wide-field fluorescence microscope. Bottom panel: Wild-type cells expressing mScarlet-D4H together with Trq-CtRac1 (PY6237) were induced with serum as in Fig 1B and images were taken with a spinning disk confocal microscope and central z-section, as well as merge images, are shown. B) Ergosterol distribution is altered in the *drs2* mutant. Images of *drs2*/*drs2* cells (*drs2*, PY6083) and *drs2*/*drs2* + *pDRS2DRS2* cells (*drs2* + *DRS2*, PY6218) expressing mScarlet-D4H were taken as in Fig 6A bottom panel.

https://doi.org/10.1371/journal.pgen.1010549.g007

polarization, determined as the apical versus sub-apical D4H signal, was also similar in these two mutants and not substantially different from that of wild-type cells. Notably, the ergosterol tip polarization was significantly reduced in the *osh4* mutant alone, which exhibits hyphal growth similar to wild-type cells, suggesting that there is not a direct correlation between ergosterol tip polarization and hyphal growth. Together, these data indicate that Drs2 *per se* is not required for hyphal invasive growth, but rather that a balance in the activities of Drs2 and Osh4 regulate this process, likely *via* regulation of the PM PI(4)P gradient.

Deletion of both *DRS2* and *SAC1* results in a synthetic growth defect

To further examine the importance of the PM PI(4)P gradient, we generated mutants deleted for the lipid phosphatase Sac1, which dephosphorylates PI(4)P, and is responsible for regulating PM PI(4)P, both in yeast and mammalian cells [64,65]. In *C. albicans*, Sac1 is critical for the steep PM PI(4)P gradient [56] and hyphal growth maintenance [56,66]. In *S. cerevisiae*, deletion of either *KES1* or *SAC1* is synthetically lethal in cells largely devoid of ER-PM contact

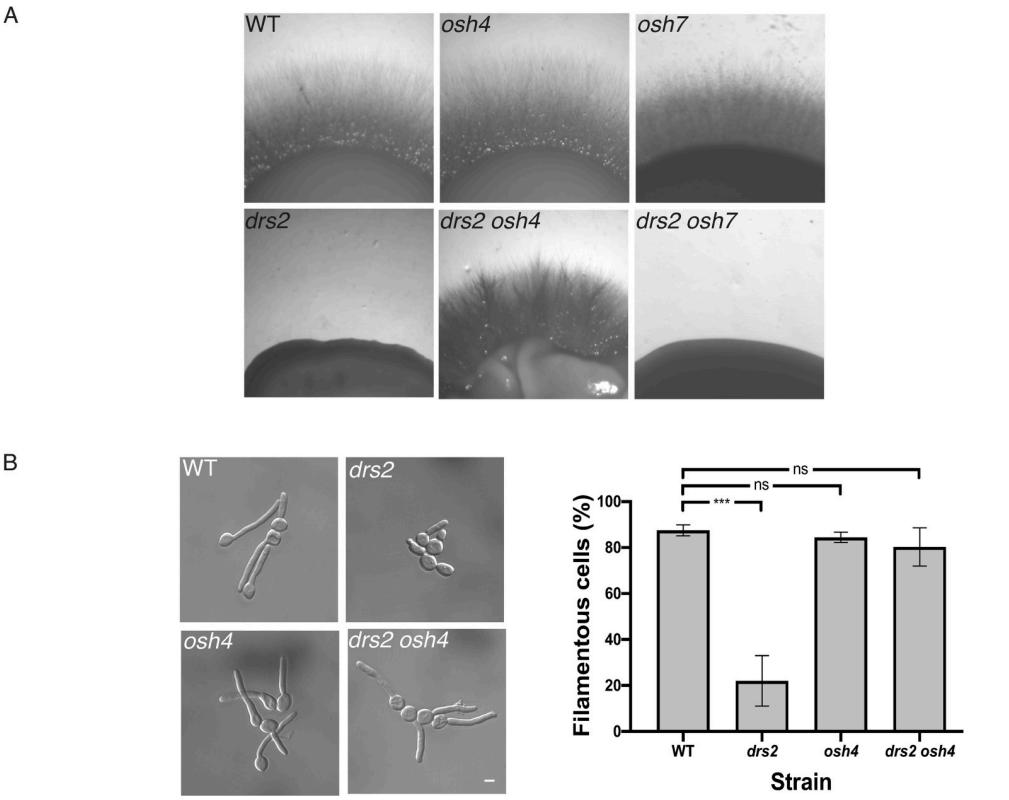

Fig 8. Deletion of *OSH4* rescues hyphal invasive growth in the *drs2* mutant. A) Invasive filamentous growth is specifically restored in the *drs2* mutant upon deletion of *OSH4*. The indicated strains, WT (PY4861), *osh4/osh4* (*osh4*, PY3974), *osh7/osh7* (*osh7*, PY5256), *drs2/drs2* (*drs2*, PY3375), *drs2/drs2 osh4/osh4* (*drs2 osh4*, PY5539) and *drs2/drs2 osh7/osh7* (*drs2 osh7*, PY5297), were grown as in Fig 1A and images were taken after 6 days. Similar results were observed in 2 independent experiments. B) Hyphal growth is restored in the *drs2* mutant upon deletion of *OSH4*. Cells from the indicated strains were incubated with serum as in Fig 1B. Bars are 5 μm. The graph represents the percentage of hyphae in the indicated strains, calculated as in Fig 1C. The percentage of hyphae was 82 ± 8%, 80 ± 6% and 76 ± 9% for the wild-type, *osh4* and *drs2 osh4* cells, respectively. ***, $P < 0.0005$; ns, not significant.

https://doi.org/10.1371/journal.pgen.1010549.g008

sites [67], and cold-sensitive growth of a *drs2* deletion mutant is partially suppressed by deletion of either *SAC1* or *KES1* [31]. As deletion of *OSH4* restored PI(4)P polarized distribution in *drs2*, as well as hyphal growth, we investigated the effect of *SAC1* deletion in the *drs2* mutant and RT-PCR confirmed the absence of *DRS2* and/or *SAC1* in the respective mutants (Fig 10A). Fig 10B and 10C show that budding growth was altered in such a *drs2 sac1* mutant, with a doubling time of 270 min compared to 90 min for WT, *drs2* and *sac1* strains. Furthermore, in serum-containing liquid media, while the *sac1* mutant formed filamentous cells, albeit shorter than the wild-type cells (Fig 10D; [56,66]), the *drs2 sac1* mutant was unable to form filamentous cells, even after 270 min incubation. Together, these data show that *DRS2* and *SAC1* show a synthetic negative interaction in *C. albicans*, indicating that they operate in parallel pathways.

Drs2 is important for plasma membrane organization

In addition to a defect in filamentous hyphal growth, the *drs2* mutant also exhibits a hypersensitivity to CFW and FCZ, compared to wild-type cells (Fig 2A). We investigated whether a balance in the activities of Drs2 and Osh4 is also critical for growth on these compounds, and, while deletion of *OSH4* in the *drs2* mutant rescued the growth defect on CFW, it did not rescue

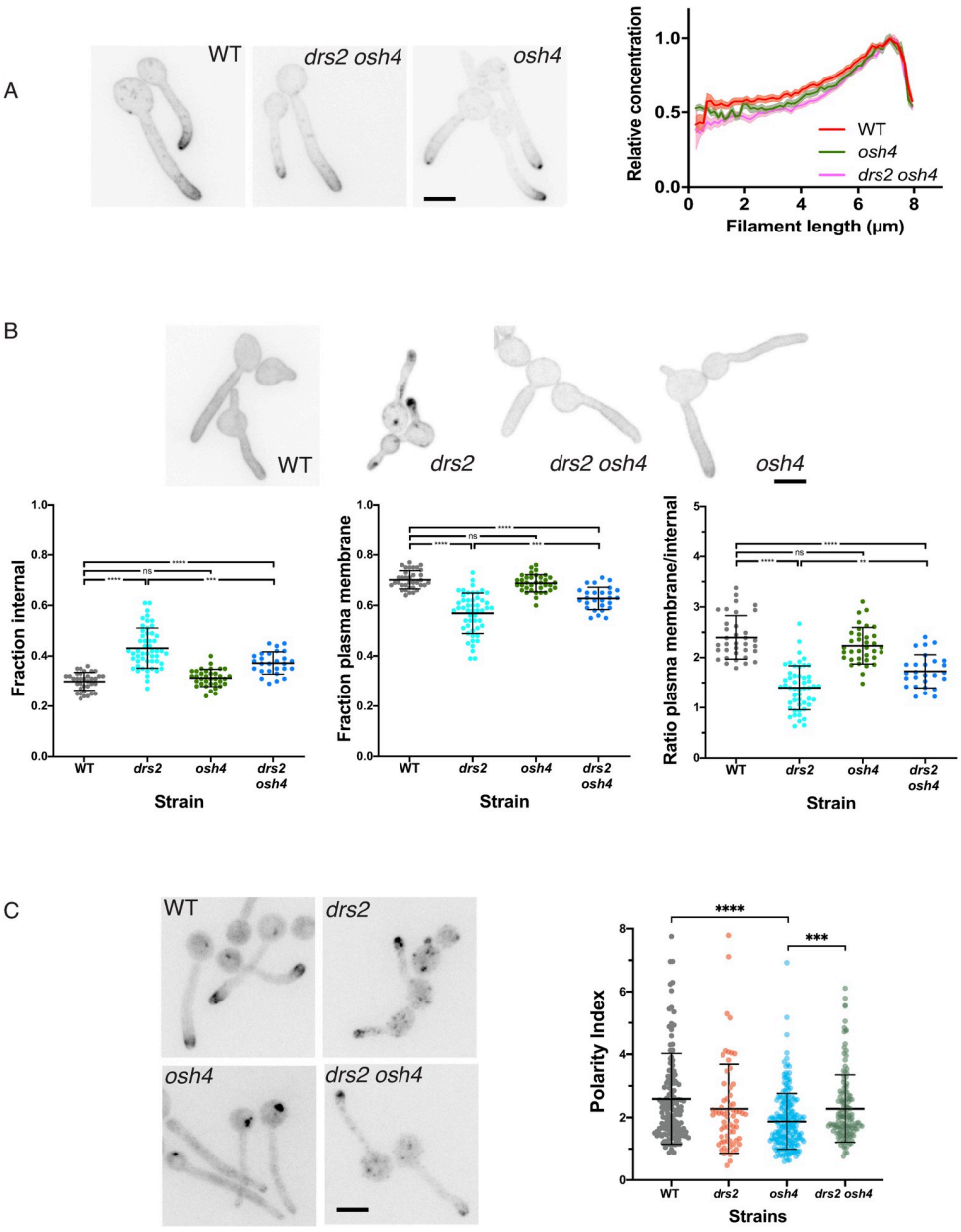

Fig 9. Deletion of *OSH4* rescues PI(4)P distribution in the *drs2* mutant. A) PI(4)P distribution is restored in the *drs2* mutant upon *OSH4* deletion. Indicated cells expressing GFP-$(PH^{OSH2[H340R]})_2$-GFP, WT (PY5619), *drs2*/*drs2 osh4*/*osh4* (*drs2 osh4*, PY5630) and *osh4*/*osh4* (*osh4*, PY5626) were incubated as in Fig 6B, with sum projections of representative cells shown. The graph illustrates the means ± the SEM of the relative concentration of PM PI(4)P as a function of filament length, normalized to the maximal signal for each cell (n = 100 cells). B) PS distribution is partially restored in the *drs2* mutant upon *OSH4* deletion. Indicated cells expressing GFP-LactC2, WT (PY3239), *drs2*/*drs2* (*drs2*, PY5134), *drs2*/*drs2 osh4*/*osh4* (*drs2 osh4*, PY5364) and *osh4*/*osh4* (*osh4*, PY5336) were incubated as in Fig 6B, with sum projections of representative cells shown. The graphs represent the relative PM and internal PS fractions, as well as the ratio of the signal at the PM over the internal signal for the indicated strains (n = 30–50 cells each), and bars mean ± the SD. ****, $P < 0.0001$; ***, $P < 0.001$; **, $P < 0.01$; ns, not significant. C) *OSH4* deletion does not substantially restore ergosterol distribution in the *drs2* mutant. Images of the indicated strains expressing mScarlet-D4H, WT (PY6037), *drs2*/*drs2 osh4*/*osh4* (*drs2 osh4*, PY6286) and *osh4*/*osh4* (*osh4*, PY6076) were taken as in Fig 7B. The graph represents the ergosterol tip polarization, *i.e.* the ratio of apical to sub-apical D4H signals, in the indicated strains.

https://doi.org/10.1371/journal.pgen.1010549.g009

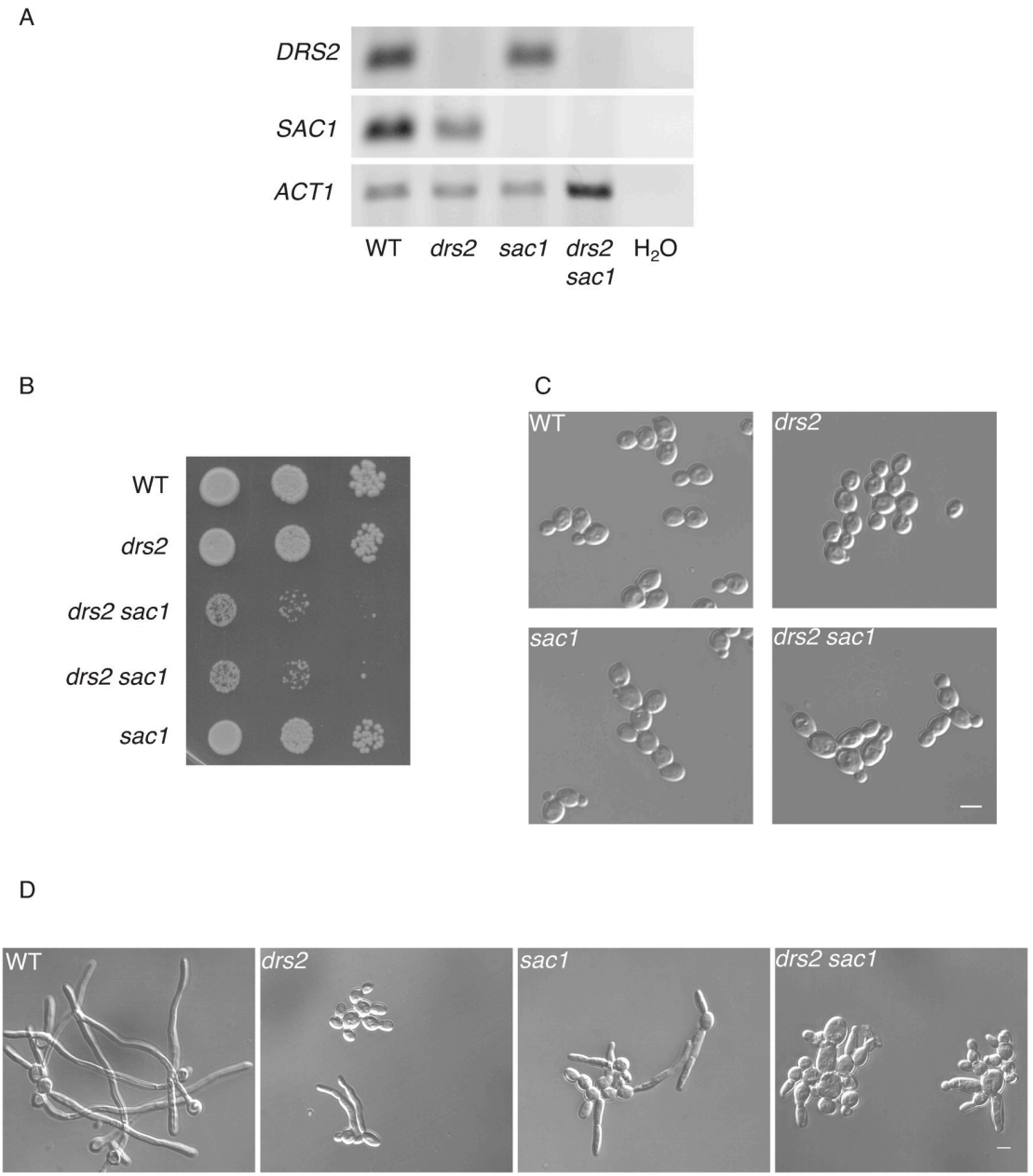

Fig 10. *DRS2* and *SAC1* interact during *C. albicans* development. A) *DRS2* and *SAC1* transcript levels. Transcripts of the indicated strains, as in Fig 9B, were determined by RT-PCR, using *SAC1*.pTm/*SAC1*.mTm (90 bp) and *DRS2*.pTm/*DRS2*.mTm (62 bp) primer pairs. B) Deletion of both *DRS2* and *SAC1* results in a synthetic growth defect. Serial dilutions of indicated strains, WT (PY4861), *drs2*/*drs2* (*drs2*, PY3375), *drs2*/*drs2 sac1*/*sac1* (*drs2 sac1*, PY6431 & PY6432) and *sac1*/*sac1* (*sac1*, PY6436), were spotted on YEPD and images were taken after 3 days. Similar results were observed in 2 independent experiments. C) Morphology of *drs2 sac1* budding cells. Cells from the indicated strains WT (PY4861), *drs2*/*drs2* (*drs2*, PY3375), *drs2*/*drs2 sac1*/*sac1* (*drs2 sac1*, PY6432) and *sac1*/*sac1* (*sac1*, PY6436), were grown to exponential phase in YEPD. D) The *drs2 sac1* mutant does not generate hyphae in response to serum. Indicated strains, as in Fig 9B, were grown in the presence of serum for 180 min. At 90 min, the percent of filamentous cells was 83 ± 5%, 19 ± 8%, 38 ± 4% and 2 ± 1% for the WT, *drs2*, *sac1* and *drs2 sac1* strains, respectively; *n* ~ 100 cells. Bars are 5 μm.

https://doi.org/10.1371/journal.pgen.1010549.g010

that on FCZ (Fig 11A). Furthermore, as the *drs2* mutant was reported to be hypersensitive to copper ions [35], we investigated whether deletion of *OSH4* could restore growth in this condition. Fig 11B shows that both *drs2* and *drs2 osh4* mutants were similarly reduced for growth on

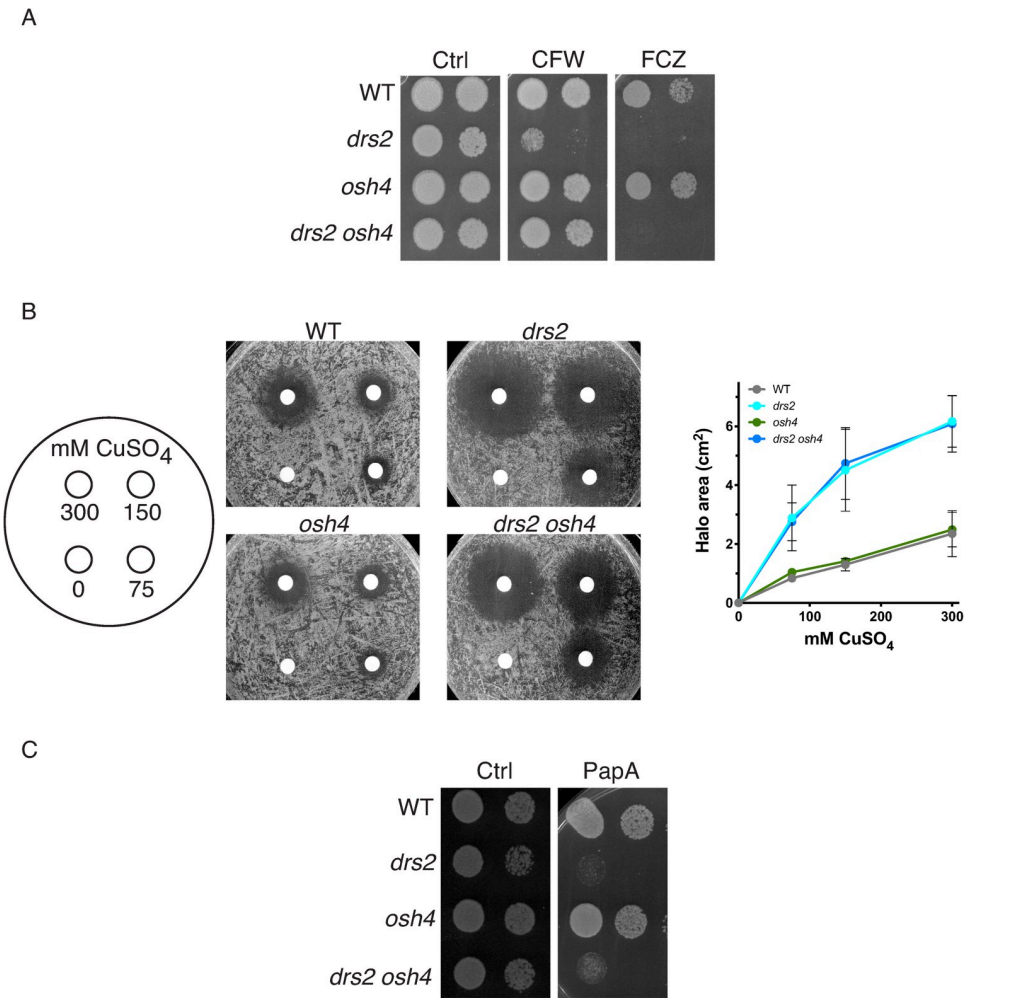

Fig 11. Deletion of *OSH4* does not rescue growth on fluconazole or copper in the *drs2* mutant. A) Deletion of *OSH4* rescues growth on calcofluor white but not that on fluconazole in the *drs2* mutant. Serial dilutions of indicated strains as in Fig 2B were spotted on YEPD media (Ctrl) containing 25 μg/ml calcofluor white (CFW) or 5 μg/ml fluconazole (FCZ). Images were taken after 2 days. Similar results were observed in 2 experiments. B) Deletion of *OSH4* does not restore growth on copper in the *drs2* mutant. The indicated strains, WT (PY4861), *drs2*/*drs2* (*drs2*, PY3375), *drs2*/*drs2 osh4*/*osh4* (*drs2 osh4*, PY5539) and *osh4*/*osh4* (*osh4*, PY3974), were spread on YEPD and filter disks contained 10 μl of 0, 75, 150, or 300 mM $CuSO_4$, were added as in [35]. The zone of growth inhibition surrounding the filter discs was recorded after 1 day at 30˚C and graphs represent averages of 3 independent experiments, with standard deviations indicated. C) Deletion of *OSH4* does not restore growth on papuamide A of the *drs2* mutant. Serial dilutions of indicated strains, WT (PY4861), *drs2*/*drs2* (*drs2*, PY3375), *drs2*/*drs2 osh4*/*osh4* (*drs2 osh4*, PY5539) and *osh4*/*osh4* (*osh4*, PY3974), were spotted on YEPD media (Ctrl) containing 1 μg/ml papuamide A (PapA) and images were taken after 2 days. Similar results were observed in 2 experiments.

https://doi.org/10.1371/journal.pgen.1010549.g011

$CuSO_4$, compared to wild-type and *osh4* cells, indicating that Drs2 has specific roles that are not linked to Osh4 activity.

As shown above, using the LactC2 reporter, we observed that the distribution of PS was altered during hyphal growth in the *drs2* mutant [36]. Papuamide A (PapA) is a depsipeptide toxin that binds PS in the outer leaflet of the PM [68]. In *C. albicans* the *cho1* deletion mutant, which lacks the PS synthase, is less sensitive to PapA than WT cells [69]. Fig 11C shows that the *drs2* mutant was hypersensitive to PapA, compared to the wild-type strain, reflecting increased PS in the PM outer leaflet. Interestingly, the *drs2 osh4* mutant did not grow on PapA, similar to *drs2*, while the *osh4* mutant grew similar to the wild-type (Fig 11C). These

results indicate that in this *drs2 osh4* mutant, the PM PS bilayer asymmetry is not re-established.

The distinct roles of Drs2 can be associated with different localizations

Our data indicate that while filamentous growth was restored in the *drs2* mutant by *OSH4* deletion, growth on fluconazole and papuamide A was not. On the other hand, Fig 5 shows that, in *C. albicans*, Drs2 localizes to different structures, including the SPK. Hence, we investigated whether a specific localization of Drs2 is critical for distinct functions, by using a synthetic physical interaction (SPI) approach to stabilize Drs2 at secretory vesicles, which accumulate at the SPK [50]. To generate a mutant with Drs2 restricted/stabilized at the SPK, we used a strain expressing a GFP nanobody (GNB) fused to one copy of Mlc1-iRFP, together with Drs2GFP as the sole expressed copy of *DRS2*. Fig 12A (bottom panel) shows that, in such a mutant, Drs2 and Mlc1 co-localized predominantly at the SPK, with the Drs2 signal strikingly increased in the strain expressing Mlc1-GNB, compared to a control strain (top panel), consistent with Drs2 stabilized at this structure. In this strain expressing Mlc1-GNB, Drs2 was not detected along the PM, compared to what we observed in the absence of the GNB construct (Figs 5 and 12A, top panel). In such a mutant expressing Mlc1-GNB, invasive filamentous growth was not altered (Fig 12B), with 85% of the cells forming hyphae in serum-containing liquid media after 90 min. In contrast, this mutant did not grow on fluconazole or papuamide A (Fig 12C). These data indicate that different roles of Drs2 are associated with its distinct cellular localizations, and suggest that *C. albicans* sensitivity to papuamide A is associated with Drs2 localization at the PM.

Given that deletion of *OSH4* restored filamentous growth in a *drs2* mutant, but not growth on fluconazole or papuamide A, we investigated the effect of recruiting Osh4 to the SPK in these growth conditions. In *S. cerevisiae*, it was shown that the majority of Osh4 was cytoplasmic, with some punctae concentrated in small buds and mother–daughter necks [70]. In *C. albicans* hyphal cells, we did not detect a distinct localization of Osh4 (Fig 13A, top left panel), similar to what was reported for the *A. nidulans* Osh4 homolog, OshC [71]. However, in cells expressing both Mlc1-GNB and Osh4-GFP, as the sole expressed copy of *OSH4*, Osh4 co-localized with Mlc1 at the SPK, indicating that Mlc1-GNB recruited this LTP (Fig 13A). Such a recruitment of Osh4 in a wild-type strain background did not alter filamentous growth, yet it restored filamentous growth in liquid media and partially restored that on solid media in a *drs2* strain background (Fig 13B). In contrast, growth on papuamide A was not restored (Fig 13C). Together, these data indicate that recruitment of Osh4 to the SPK has a similar affect as deleting *OSH4* in *drs2* cells for filamentous growth.

Discussion

Our results show that Drs2 is critical for *C. albicans* invasive filamentous growth and that a *drs2* deletion mutant exhibits increased sensitivity to calcofluor white and fluconazole, as well as papuamide A. The *drs2* mutant also has an altered PS, PI(4)P and ergosterol distribution, but not that of $PI(4,5)P_2$. The requirement for Drs2 in invasive filamentous growth, as well as growth in the presence of the chitin binding dye calcofluor white, can be specifically bypassed by the deletion of the lipid transfer protein Osh4, but not by that of other Osh proteins. Deletion of *OSH4* in *drs2* also restores the PI(4)P distribution and significantly the PS distribution, but not growth on papuamide A. Given that papuamide A binds PS in the outer leaflet of the PM, this indicates that the level of PS in the PM outer leaflet remains altered. In *C. albicans*, Drs2 localizes to different compartments, *i.e.* the Golgi, the Spitzenkörper and the PM. Such a localization of Drs2 is reminiscent of that of ChsB and SynA in *A. nidulans* [72], suggesting

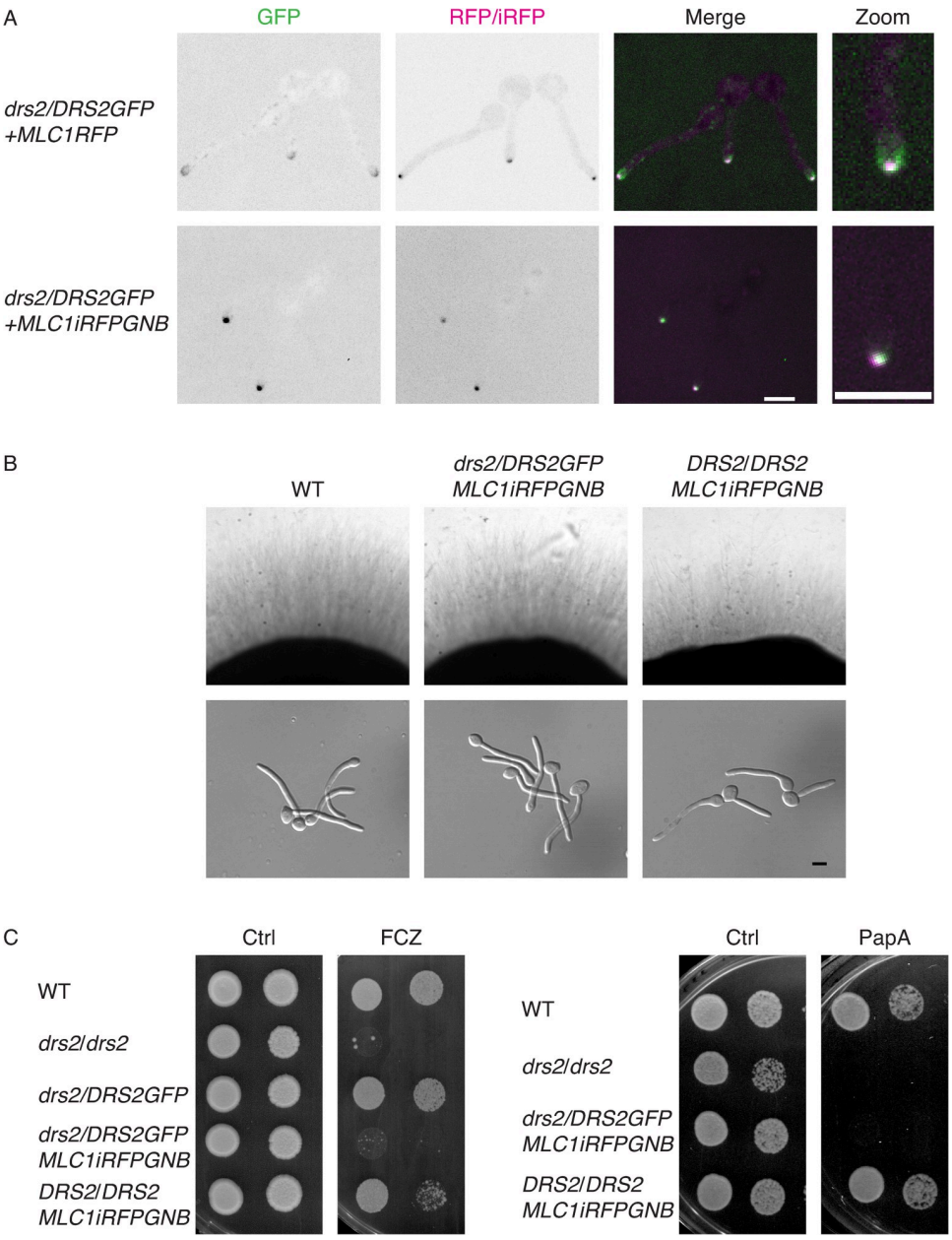

Fig 12. Stabilization of Drs2 at the Spitzenkörper alters growth on papuamide A and fluconazole. A). Synthetic physical interaction (SPI) between Drs2 and Mlc1 stabilizes Drs2 at the Spitzenkörper. Representative images (central z-sections) of cells expressing Drs2-GFP, as a sole copy of Drs2, with either Mlc1RFP (PY4928) or Mlc1-iRFP-GNB (PY5885) are shown; iRFP stands for near-*i*nfrared *f*luorescent *p*rotein and GNB for GFP nanobody. Right panels are enlargement of merge images. B) Stabilization of Drs2 at the SPK does not alter invasive filamentous growth. The indicated strains, WT (PY4861), *drs2/DRS2GFP MLC1-iRFP-GNB* (PY5885) and *DRS2/DRS2 MLC1-iRFP-GNB* (PY5385) were grown on agar-containing serum media and images were taken after 6 days (top panels) or grown in the presence of serum for 90 min (bottom panels). The percent of filamentous cells was 85–86% for the wild-type, *drs2/DRSGFP MLC1-iRFP-GNB* and *DRS2/DRS2 MLC1-iRFP-GNB* strains; 2 experiments, $n \sim 100$ cells. C) Stabilization of Drs2 at the SPK alters growth on fluconazole and papuamide A. Serial dilutions of WT (PY4861), *drs2/drs2* (PY3375), *drs2/DRS2GFP* (PY4665), *drs2/DRS2GFP MLC1-iRFP-GNB* (PY5885) and *DRS2/DRS2 MLC1-iRFP-GNB* (PY5385) strains spotted on YEPD media (Ctrl) containing either 2.5 μg/ml fluconazole (FCZ) or 2 μg/ml papuamide A (PapA) and images were taken after 2 days.

https://doi.org/10.1371/journal.pgen.1010549.g012

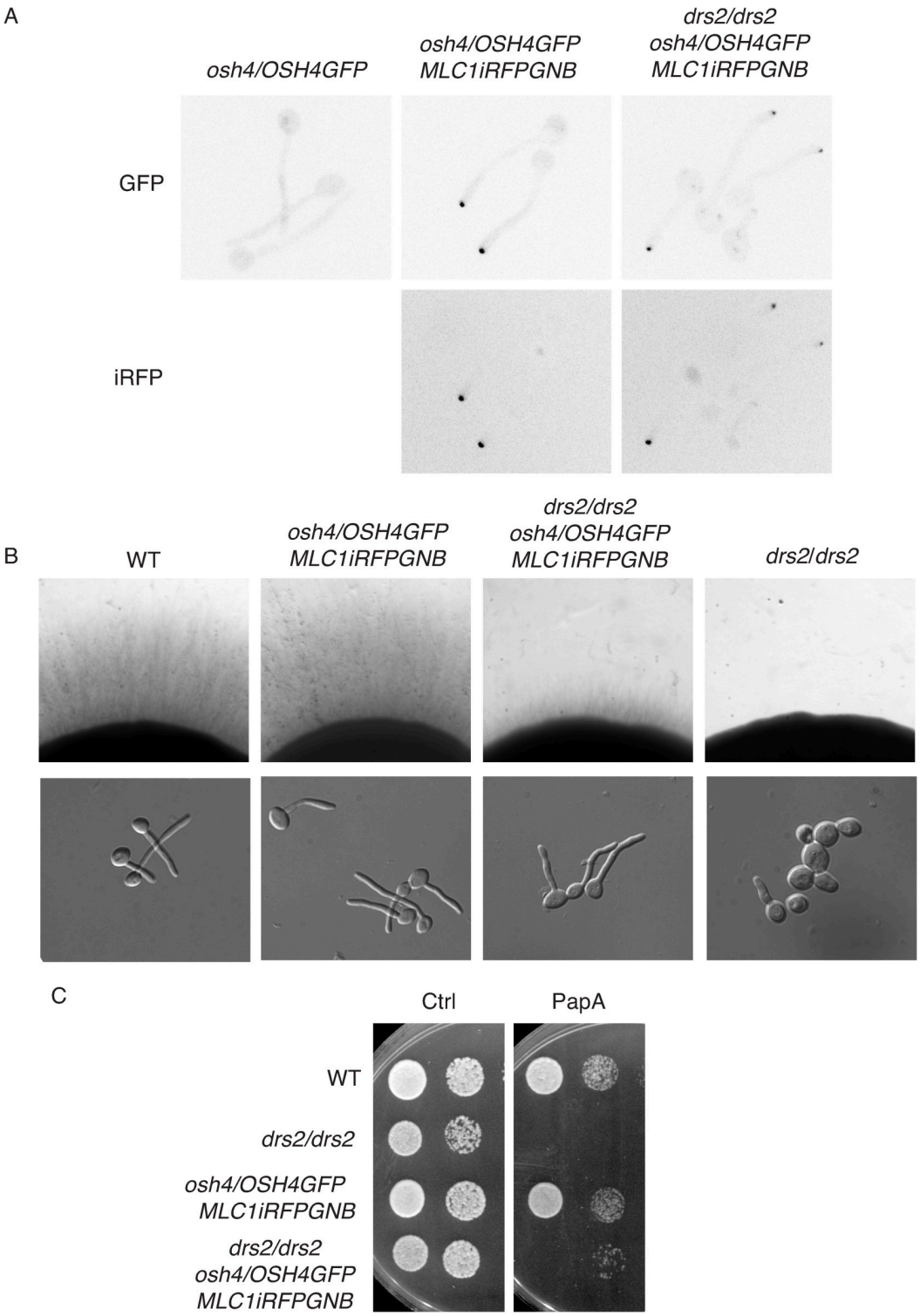

Fig 13. The recruitment of Osh4 to the Spitzenkörper in *drs2* phenocopies *drs2 osh4*. A). Synthetic physical interaction between Osh4 and Mlc1 recruits Osh4 to the Spitzenkörper. Representative images (Max projections) of cells expressing Osh4-GFP, as a sole copy of Osh4, without (PY5875) or with Mlc1-iRFP-GNB, in the wild-type (PY5931) or the *drs2* deletion (PY6447) strains are shown. B) Recruitment of Osh4 at the SPK restores invasive filamentous growth in a *drs2* deletion strain. Indicated strains, wild-type (PY4861), *drs2/drs2* (PY3375), *drs2/drs2 osh4/OSH4GFP MLC1-iRFP-GNB* (PY6447) and *DRS2/DRS2 osh4/OSH4GFP MLC1-iRFP-GNB* (PY5931) were grown on agar-containing YEPD with serum and images were taken after 6 days (top panels) or grown in the presence of serum for 90 min (bottom panels). At 90 min,

the percent of filamentous cells was on average 85%, 78%, 78% and 22% for PY4861, PY5931, PY6447 and PY3375 strains, respectively; 2–3 independent experiments with $n \sim 100$ cells. C) Recruitment of Osh4 at the SPK does not restore growth on papuamide A in the *drs2* mutant. Serial dilutions of indicated strains as in Fig 13B, were spotted on YEPD media (Ctrl) containing 2μg/ml papuamide A (PapA) and images were taken after 2 days.

https://doi.org/10.1371/journal.pgen.1010549.g013

that this flippase also follows the endocytic recycling pathway. We propose that distinct roles of Drs2 are associated with different localizations.

Role of Drs2 in plasma membrane organization

In *S. cerevisiae*, it was shown that the *DRS2/DNF1-3* genes have some redundancy during budding growth [20]. Similarly, in the filamentous fungus *A. nidulans*, a double deletion of the Dnf1 and Drs2 homologs (DnfA and DnfB, respectively) is lethal [25,73], indicating that these flippases are redundant, in particular for growth. Yet, they appear to also have unique functions and/or localizations in different fungi. For example, in contrast to the case in *C. albicans*, deletion of the Drs2 homolog DnfB alone does not drastically alter *A. nidulans* hyphal growth [25]. With respect to localization, Drs2 is associated to the Golgi apparatus in *S. cerevisiae*, even in shmoos [24], while its homolog in *A. nidulans* DnfB localizes to the SPK [25]. We show here that CaDrs2 localizes to the filament apex (SPK and PM), in addition to the Golgi apparatus, and our data indicate that these distinct localizations are associated with different Drs2 functions. Indeed, upon stabilization of Drs2 at secretory vesicles that accumulate at the SPK, in which this flippase is no longer detected at the PM, cells are similar to that of the wild-type for invasive filamentous growth and calcofluor white sensitivity, yet unable to grow on papuamide A. Furthermore, deletion of Osh4, which restores hyphal growth and calcofluor white sensitivity, does not restore *drs2* growth on papuamide A, hence the level of PS in the PM external leaflet. Copper binds PS with high affinity and a *drs2* mutant is hypersensitive to copper, linking PS and copper sensitivity [35]. Given that *drs2 osh4* grows similar to *drs2* on copper and papuamide A, we suggest that Drs2 is required for regulating PS asymmetry, *via* its ability to flip PS across the PM.

Role of lipids in invasive filamentous growth

A *drs2* deletion mutant is defective in invasive filamentous growth in response to serum, and deletion of *OSH4* can specifically overcome these defects. Upon serum exposure, the *drs2* cells exhibit an alteration in the PM lipid distribution, *i.e.* PS, PI(4)P and ergosterol, which is at least partially compensated by *OSH4* deletion, raising the question of the respective contribution of these lipids to hyphal growth.

Sterol-rich membrane domains, have been visualized, by using filipin, at the tips of mating projections in *S. cerevisiae* [74], at cell poles and division site in *S. pombe* [75], as well as at the hyphal tips of *C. albicans* [58] and *A. nidulans* [76], where they are thought to contribute to polarized growth. In *S. cerevisiae drs2* cells, 20% of ergosterol appears to mislocalize to internal membranes, as assessed by filipin staining and DHE fluorescence, and deletion of *KES1* suppresses the accumulation of intracellular ergosterol in this *drs2* mutant [77]. Our data, using the D4H reporter for free ergosterol within the cell, indicates that 96 ± 7% and 78 ± 12% of cells had multiple internal punctae in the *drs2* and *drs2 osh4* mutants, respectively, compared to 1 ± 2% and 9 ± 6% in wild-type and *osh4* cells, respectively, indicating that removal of Osh4 did not substantially suppress internal ergosterol accumulation in *C. albicans drs2* cells. Polarization of ergosterol to the growth tip also appears similar in the *drs2* and *drs2 osh4* mutants, at a level intermediate between the wild-type and *osh4* cells. Whether this polarized ergosterol signal is associated with the tip crescent and/or the SPK is unclear. In *S. pombe*, ergosterol

associated D4H internal signals, which are enriched upon Arp2/3 inhibition, correspond to membrane-enclosed compartments, referred to as sterol-rich compartments [62]. Both this ergosterol movement to internal structures and the anterograde transport appear to be independent of vesicular trafficking [62]. Although the mechanism of sterol transfer is still to be determined, it is unlikely that the filamentous growth defect in *drs2* directly results from the observed alteration of ergosterol distribution.

In *C. albicans*, the phosphatidylinositol 4-kinase *stt4* deletion mutant, in which PM PI(4)P is no longer detectable, and the PS synthase *cho1* mutant, which has little to no PS, exhibit defective filamentous growth and increased sensitivity to the antifungal drug caspofungin [9,78]. Both these mutants have increased exposure of cell wall β(1,3)-glucan and, given that 50% of PS is still detectable at the PM of *stt4*, we proposed that PM PI(4)P levels are associated with virulence by masking of cell wall β(1–3)-glucan [78]. In contrast to these mutants, the *drs2* mutant grows similar to the wild-type cells on caspofungin and congo red, making it unlikely that the glucan synthase pathway is affected. As PM PS and PI(4)P levels are not drastically altered compared to the *cho1* and *stt4* deletion mutants, why the virulence is altered in *drs2* is unclear. Similar to the *drs2* mutant, the ratio of mean PM PS to internal PS decreases in a *C. albicans stt4* mutant, with increased internal PS levels compared to wild-type cells [78], yet, as for *stt4*, our results are inconsistent with a correlation between PS distribution and filamentous growth defect in the *drs2* mutant. Indeed, while invasive filamentous growth was restored upon deletion of Osh4, the PM to internal PS ratio was only partially restored, and deletion of Osh4 did not restore growth on papuamide A. Rather, PM PI(4)P appears to be critical. In *S. cerevisiae*, the cold-sensitive growth of a *drs2* deletion mutant is partially suppressed by deletion of either the Osh4 homolog, Kes1, or the PI(4)P phosphatase Sac1 [31]. In *C. albicans*, deletion of Sac1 results in cells with altered PM PI(4)P gradient, as well as filamentous growth [56,66]. While the apical PI(4)P gradient as well as filamentous growth are restored upon deletion of Osh4 in *drs2* cells, deletion of Sac1 substantially affects growth in *drs2*, presumably by increasing the level of PM PI(4)P. Together, these results strongly suggest that the PM PI(4)P gradient, rather than the level of PI(4)P, is critical for filamentous growth.

Role of Drs2 in cell wall integrity and fluconazole sensitivity

Lipid transport through vesicular and non-vesicular trafficking is well established [79] and PS flipping activity of Drs2 is critical for the vesicular transport of a number of PM proteins. For example, ScDrs2 is required at the Golgi for efficient segregation of cargo into exocytic vesicles, as the PM proteins Pma1 and Can1 are missorted to the vacuole in *drs2* cells, and deletion of *KES1* suppresses this defect [77]. Hence, it is likely that the hypersensitivity of the *drs2* mutant both for calcofluor white and fluconazole results from an alteration of membrane traffic in specific pathways. Interestingly, the *drs2* mutant exhibits increased sensitivity to calcofluor white but not to caspofungin, suggesting that the chitin synthase pathway is selectively altered. Consistently, it was proposed that PS translocation to cytosolic leaflet of the Golgi by a flippase is critical for the *S. cerevisiae* chitin synthase (Chs3) trafficking [80]. The growth defect of *drs2* on fluconazole may result from a mislocalization of multi-drug transporters [39] and, consistent with such a scenario, we observe that ~ 80% of the *drs2* cells had internal Cdr1 signal (Fig 2C). It would be interesting to investigate the importance of this flippase in pathogenic non *albicans Candida* species, known for their resistance to the antifungal drug, such as *C. glabrata* or *C. auris* [81].

Altogether our results are consistent with the notion that in *C. albicans* Drs2 down-regulates Osh4 activity, similar to *S. cerevisiae* [77], as wild-type filamentous growth and cell wall integrity were rescued in *drs2*, either by deleting or targeting Osh4 to the SPK. Furthermore,

our data suggest that Osh4 does not function together with Drs2 at the SPK for filamentous growth, as targeting Osh4 to this organelle has the same effect as deleting Osh4. Strikingly, our data show that the genetic interaction between homologs of two different lipid transporters identified in *S. cerevisiae* budding growth [31], occurs during hyphal growth, a distinct growth mode in filamentous fungi. *C. albicans* diverged from *S. cerevisiae* ~250 million years ago [82], hence an attractive possibility is that such an interaction is a conserved feature of the fungal kingdom, and filamentous fungi, with a large diversity in size and growth rate, represent useful models to understand how membrane expansion is regulated by lipid transport mechanisms.

Materials and methods

Ethics statement

Animal procedures were approved by the Bioethical Committee and Animal Welfare of the Instituto de Salud Carlos III (CBA2014_PA51) and of the Comunidad de Madrid (PROEX 330/14) and followed the current Spanish legislation (Real Decreto 53/2013) along with Directive 2010/63/EU.

Growth conditions

Yeast extract-peptone dextrose (YEPD) or synthetic complete (SC) medium was used and strains were grown at 30˚C, unless indicated otherwise. Filamentous growth induction was carried out as described previously either with 50% serum in liquid media and agar plates, or 75% on agarose pads for microscopy [83]. For filipin staining experiments, 10% of serum was used. Growth on YEPD plates containing Congo red, calcofluor white, caspofungin or fluconazole was examined as described [84]. Copper sensitivity was investigated as described [30]. Congo red, calcofluor white, filipin, hygromycin and fluconazole were from Fluka, Sigma-Aldrich, Saint Quentin Fallavier, France. Papuamide A was from University British Columbia.

Strains and plasmids

Strains and oligonucleotides used are listed in Tables 1 and 2, respectively. All strains were derived from BWP17 [85]. The deletion mutants were generated by homologous recombination. Each copy was replaced by either *HIS1*, *URA3*, *ARG4*, *SAT1* or *HYGB*, using knockout cassettes generated by amplification of pGem-*HIS1*, pGem-*URA3*, pGem-*CdARG4*, pFa-*ARG4*, pFa-*SAT1* and pBH1S [85–88] with primer pairs *DNF1.P1/DNF1.P2*, *DNF2.P1/DNF2.P2*, *DNF2.P3/DNF2.P4 DNF3.P1/DNF3.P2*, *OSH4.P1/OSH4.P2*, *OSH7A.P1/OSH7A.P2*, *OSH7α.P1/OSH7α.P2*, *OSH2.P1/OSH2.P2*, *OSH3.P1/OSH3.P2* and *SAC1.P1/SAC1.P2*. The *drs2Δ/drs2Δ osh4Δ/osh4Δ*, *drs2Δ/drs2Δ osh2Δ/osh2Δ*, *drs2Δ/drs2Δ osh3Δ/osh3Δ*, *drs2Δ/drs2Δ osh7AΔ/osh7αΔ* and *drs2Δ/drs2Δ sac1Δ/sac1Δ* strains were generated from the *drs2Δ/drs2Δ* strain (PY3310 [36]) and the *dnf1Δ/dnf1Δ dnf2Δ/dnf2Δ* strain from the *dnf2Δ/dnf2Δ* strain (PY5804).

Plasmid *pDUP3-pADH1DNF2* was constructed by amplification from gDNA of the *DNF2* ORF, using primers with a unique AscI site at the 5' end (DNF2.P5) and a unique MluI site at the 3' end (DNF2.P6) and *pDUP3-pDRS2DRS2* by amplification from *pExp-pDRS2DRS2* [36] of the *DRS2* ORF together with 1 kb upstream and downstream, using primers with a unique SpeI site at the 5' end (*DRS2.P1*) and a unique NotI site at the 3' end (*DRS2.P2*). The fragments were subsequently cloned into *pDUP3-SAT1* [89], yielding to *pDUP3-pADH1DNF2* and *pDUP3-pDRS2DRS2*, respectively. To visualize Drs2, Dnf2 and Osh4, GFPγ was inserted by homologous recombination at the 3' end of *DRS2*, *DNF2* or *OSH4* ORF in strains heterozygous

Table 1. Strains used in the study.

STRAIN	RELEVANT GENEOTYPE	REFERENCE
BWP17	*ura3Δ::λimm434/ura3Δ::λimm434 his1Δ::hisG/his1Δ::hisG arg4::hisG/arg4Δ::hisG*	[85]
PY1206	Same as BWP17 with *RP10::ARG4-pADH1*-GFP-$PH^{PLC\delta1}$-$PH^{PLC\delta1}$-GFP	[57]
PY2263	Same as BWP17 with *RP10::ARG4 pACT1-CRIBGFP*	[48]
PY2578	Same as BWP17 with *RP10::pADH1-FAPP1*$^{[E50A,H54A]}$*GFP*	[56]
PY3239	Same as BWP17 with *RP10::ARG4- pACT1GFP-yeLactC2*	[36]
PY3310	Same as BWP17 with *drs2Δ::HIS1/ drs2Δ::URA3*	[36]
PY3375	Same as PY3310 with *RP10::ARG4*	[36]
PY3873	Same as PY3310 with *RP10::pADH1-FAPP1*$^{[E50A,H54A]}$*GFP*	[56]
PY3921	Same as BWP17 with *osh4Δ::URA3/ osh4Δ::HIS1*	This study
PY3945	Same as BWP17 with *osh3Δ::HIS1/ osh3Δ::URA3*	This study
PY3974	Same as PY3921 with *RP10::ARG4*	This study
PY3977	Same as PY3945 with *RP10::ARG4*	This study
PY3995	Same as BWP17 with *osh2Δ::HIS1/ osh2Δ::URA3*	This study
PY4002	Same as PY3995 with *RP10::ARG4*	This study
PY4050	Same as PY3310 with *RP10::ARG4-pADH1*-GFP-$PH^{PLC\delta1}$-$PH^{PLC\delta1}$-GFP	This study
PY4665	Same as PY3303 (URA3) with *DRS2:: DRS2-GFPγ-HIS1*	This study
PY4671	Same as PY3310 with *drs2Δ::HIS1/ drs2Δ::SAT1*	This study
PY4861	*ura3Δ::λ imm434/ura3Δ::λ imm434 his1::hisG/HIS1::his1::hisG arg4::hisG/URA3::ARG4::arg4::hisG*	[83]
PY4928	Same as PY4665 with *MLC1 /MLC1-mScarlet-ARG4*	This study
PY4946	Same as BWP17 with *dnf1Δ::SAT1/ dnf1Δ::HYGB*	This study
PY4972	Same as PY3310 with *RP10:: ARG4 pACT1-CRIBGFP*	This study
PY5003	Same as PY3375 with *NEUT5L::SAT1- pADHDNF2*	This study
PY5005	Same as PY4861 with *NEUT5L::SAT1- pADHDNF2*	This study
PY5042	Same as PY3310 with *RP10::ARG4-pDRS2DRS2*	[36]
PY5134	Same as PY3310 with *NEUT5L::SAT1-pACT1GFP-yeLactC2*	This study
PY5218	Same as PY4676 with *MLC1/MLC1-mScarlet-ARG4*	This study
PY5246	Same as BWP17 with *osh7aΔ::SAT1/ osh7αΔ::HIS1*	This study
PY5256	Same as PY5246 with RP10::*URA3-ARG4*	This study
PY5296	Same as PY4671 with *osh4Δ::URA3/ osh4Δ::HYGB*	This study
PY5297	Same as PY4671 with *osh7αΔ::HYGB/osh7aΔ::URA3*	This study
PY5336	Same as PY3921 with *RP10::ARG4- pACT1GFP-yeLactC2*	This study
PY5349	Same as PY4677 with *MLC1/MLC1-mScarlet-ARG4*	This study
PY5364	Same as PY5296 with *RP10::ARG4- pACT1GFP-yeLactC2*	This study
PY5385	Same as BWP17 with *MLC1/MLC1-miRFP670-GNB-URA3*	[50]
PY5539	Same as PY5296 with *RP10::ARG4*	This study
PY5568	Same as PY3310 with *RP10::ARG4- pADH1-* GFP-$(PH^{OSH2[H340R]})_2$-GFP	This study
PY5613	Same as BWP17 with *CDC10/CDC10::CDC10-mScarlet-ARG4* and *NEUT5L::SAT1-pADH1miRFP670CtRac1*	This study
PY5615	Same as PY3310 with *CDC10/CDC10::CDC10-mScarlet-ARG4* and *NEUT5L::SAT1-pADH1miRFP670CtRac1*	This study
PY5619	Same as BWP17 with *RP10::ARG4-pADH1-* GFP-$(PH^{OSH2[H340R]})_2$-GFP	[56]
PY5626	Same as PY3921 with *RP10::ARG4- pADH1-* GFP-$(PH^{OSH2[H340R]})_2$-GFP	This study
PY5630	Same as PY5296 with *RP10::ARG4- pADH1-* GFP-$(PH^{OSH2[H340R]})_2$-GFP	This study
PY5677	Same as BWP17 with *DNF2Δ::HIS1/ DNF2*	This study
PY5741	Same as BWP17 with *dnf3Δ::URA3/ dnf3Δ::SAT1*	This study
PY5746	Same as PY5677 with *DNF2::DNF2-GFPγ-URA3*	This study
PY5801	Same as PY5741 with *RP10::ARG4-pExp and his1Δ::HIS1*	This study
PY5804	Same as BWP17 with *dnf2Δ::HIS1/ dnf2Δ::ARG4*	This study

(*Continued*)

Table 1. (Continued)

STRAIN	RELEVANT GENEOTYPE	REFERENCE
PY5814	Same as PY5804 with *NEUT5L::URA3*	This study
PY5875	Same as BWP17 with *osh4Δ::URA3/ OSH4-GFPγ-ARG4*	This study
PY5885	Same as PY5385 with *drs2Δ::CdARG4/DRS2-GFPγ-HIS1*	This study
PY5919	Same as PY5814 with *NEUT5L::SAT1-pADHDNF2*	This study
PY5922	Same as PY5871 with *NEUT5L:: SAT1-pADHDNF2*	This study
PY5931	Same as PY5385 with *osh4Δ::HYGB/ OSH4-GFPγ-ARG4*	This study
PY6037	Same as BWP17 with *RP10::ARG4- pACT1-mScarlet-D4H*	This study
PY6076	Same as PY3921 with *RP10::ARG4- pACT1-mScarlet-D4H*	This study
PY6083	Same as PY3310 with *RP10::ARG4- pACT1-mScarlet-D4H*	This study
PY6213	Same as PY6083 with *NEUT5L:: pACT1-Turquoise-CtRAC1-SAT1*	This study
PY6218	Same as PY6083 with *NEUT5L::SAT1-pDRS2DRS2*	This study
PY6235	Same as PY4946 with *RP10::ARG4*	This study
PY6237	Same as PY6037 with *NEUT5L::pACT1-Turquoise-CtRAC1-SAT1*	This study
PY6239	Same as PY5746 with *NEUT5L:: mScarlet-CtRAC1-SAT1*	This study
PY6241	Same as PY4665 with *NEUT5L:: mScarlet-CtRAC1-SAT1*	This study
PY6286	Same as PY6083 with *osh4Δ::HYGB/ osh4Δ::SAT1*	This study
PY6350	Same as PY4972 with *drs2Δ::HIS1/ drs2Δ::SAT1*	This study
PY6389	Same as PY6350 with *MLC1/MLC1-mScarlet-URA3*	This study
PY6393	Same as PY4861 with *CDR1/CDR1::CDR1-GFP-SAT1*	This study
PY6395	Same as PY3375 with *CDR1/CDR1::CDR1-GFP-SAT1*	This study
PY6400	Same as PY5804 with *dnf1Δ::URA3/ dnf1Δ::HYGB*	This study
PY6407	Same as PY5568 with *NEUT5L::SAT1-pDRS2DRS2*	This study
PY6408	Same as PY4671 with *osh2Δ::URA3/ osh2Δ::HYGB*	This study
PY6431	Same as PY4671 with *osh3Δ::URA3/ osh3Δ::ARG4*	This study
PY6432	Same as PY4671 with *sac1Δ::ARG4/ sac1Δ::HYGB*	This study
PY6436	Same as BWP17 with *sac1Δ::ARG4/ sac1Δ::HYGB*	This study
PY6447	Same as PY4671 with *osh4Δ::HYGB/ OSH4- GFPγ-ARG4* and *MLC1/MLC1-miRFP670-GNB-URA3*	This study
PY6450	Same as PY2263 with *MLC1/MLC1-mScarlet-ARG4*	This study
PY6646	Same as PY5042 with *CDR1/CDR1::CDR1-GFP-SAT1*	This study

https://doi.org/10.1371/journal.pgen.1010549.t001

for these genes, after amplification of GFPγ from the plasmid *pFA-GFPγ-HIS1* [90], using the primers *DRS2.P3/DRS2.P4*, *DNF2.P7/DNF2.P8* or *OSH4.P3/OSH4.P4*. *pExp-pACT1CRIBGFP* [48] was used to transform the WT (BWP17) and *drs2/drs2* (PY3310) strains. Cdr1-GFP, PH-FAPP1$^{[E50A,H54A]}$-GFP, GFP-(PH$^{OSH2[H340R]}$)$_2$-GFP and GFP-PHPLCδ1-PHPLCδ1-GFP expressing strains were generated as described [56,57]. pDUP5-mScarlet-CtRac1 [91] was used to transform the *drs2/DRS2GFP* (PY4665) and *dnf2/DNF2GFP* (PY5746) strains. Mlc1-mScarlet and Cdc10-mScarlet were generated by amplification of mScarlet-ARG4 from pFA-mScarlet-ARG4 [92], using the primer pairs *MLC1.P1/MLC1.P2* and *CDC10.P1/CDC10.P2*, respectively. mTurquoise-CtRac1 (mTrq-CtRac1) was constructed by replacing mScarlet in *pDUP5-pADH1-mScarlet-CtRac1* [91] with mTrq, and subsequently cloning mTrq-CtRac1 into *pDUP3*. To visualize the distribution of phosphatidylserine, a fusion of GFP with the discoidin-like C2 domain of lactadherin (GFP-LactC2) was used, as previously described [36]. Strains expressing Mlc1-iRFP-GNB were generated by homologous recombination, using pFA-iRFP670-GNB-URA3, as in [50]. To visualize the distribution of ergosterol, we used filipin staining, as described [58], as well as the genetically encoded biosensor D4H [62]. D4H was amplified from plasmid pSM2244 [62], using primer pair D4H.P1 and D4H.P2 and cloned

Table 2. Primer sequences.

PRIMER	SEQUENCE
DNF1.P1	CAAGTGACAACTCTCCAGTTAGCTCCTATTATTTGCATCGACCAAATCTAGAAGATCTTACTAGAACATCGAAAGTTGGAGTGACCATTTGCTGAAGCTTCGTACGCTGCAGGTC
DNF1.P2	CGAAAAATGTAAAACCGAAATCAAATGCAATGATACAATAAACTGAAACCCAATTACCACATAAAGTAGGTTAAGGATTCAAAGCTACACTATTCCTCTGATATCATCGATGAATTCGAG
DNF2.P1	CACCTAATTCTACTTTATCCAATTTCGAATTGCTATCCACACTCTTATGACTAAAAATAAGCACAATTTCACGCGAAGCTTCGTACGCTGCAGGTC
DNF2.P2	CTTGTATGTGTGTTTGTTGTCTATAATGTTTTCTTTTATGTTATGCAAATGAAAATTGCTGTTAATTCATTGAAGATACTCTCTGATATCATCGATGAATTCGAG
DNF2.P3	CACCTAATTCTACTTTATCCAATTTCGAATTGCTATCCACACTCTTATGACTAAAAATAAGCACAATTTCACGCTAAATAATAGTAGTGATGGAGTGTGGAATTGTGAGCGGATA
DNF2.P4	GTATGTGTGTTTGTTGTCTATAATGTTTTCTTTTATGTTATGCAAATGAAAATTGCTGTTAATTCATTGAAGATACTCTTTTTTGATTTTCGTAGCTTATTCTAGATGCTCTTTCCCAGTCACGACGTT
DNF3.P1	CTACAGATTCAACTTTATAGAATCCTACATTGAGTCACCTGTCTCATCATTTGGTCATTAATTTACAACTACAGTGAATCATACAATTAGATTTGGAAGCTTCGTACGCTGCAGGTC
DNF3.P2	GCTCGGGTGAATTGAGACAATTTTGATGTATCTTGTATATTTGTATAAATACTTAGATGTACATTTCTTTTGGTTTTGGAAACTCAATAGACACCTCTGATATCATCGATGAATTCGAG
OSH4.P1	CTATATTTTAAAATAACACATCGTCTTCAAGCCAACAGTATATTTTTTTGTCATGTCAAACTCCAAATCCAGTTCTGAAGTGTGGAATTGTGAGCGGATA
OSH4.P2	GATGTACTACTATTATAAACATTATTTTACGAAATTGAAAAAACCTACTCTAAATTCATTTAAAAGACTATTTCTTTCCCAGTCACGACGTT
OSH7A.P1	CCCTTCCATTAAATCTCCCTGAGATTTGTTGTTTTTTATCTGTATTCAGTACGAAGTCAAGTTCACCATGGGTTTAACTGTGGAATTGTGAGCGGATA
OSH7A.P2	CGATTTCTAATCTAAACTAAAGATAAATATATAAAGAAGTACATTAAATTGCAATATATCAAAAACGAATTAAGTTTCTTCTTTCCCAGTCACGACGTT
OSH7F061.P1	CCAGCGAACATGCACTTTTCTTTCGTTGAAGGTTCAGGTAATCAGTATGGGATTAACAGCTAAATTAGATAAGTGTGGAATTGTGAGCGGATA
Osh7F061.p2	TAAATTAGACAATACTACTTGATTCTAATTCAAAATCTATTAATATGACCGTATATTAAAAGTCCAACAATTAATTACTTTCCCAGTCACGACGTT
OSH2.P1	CCATAATAAATTACTGATAAAACACTAACAACTTTAGAATAAACAGCTAAAATCATGAATGATTCACCCCAACTAAGTGCGAAGCTTCGTACGCTGCAGGTC
OSH2.P2	CAATCAACAATTAAAACAGTCTAAAATATGTCTCCCGTGTTCGCCAAATCTTGTGCCTTTCTTCTAGGCCAATACTCTGATATCATCGATGAATTCGAG
OSH3.P1	CCCACTCAATCCCATTATTTCTTTCCCTTGACAGTTGAACTTTCCCATACCAACTTGAAATATGGAAACTTTAGAAGGAAGCTTCGTACGCTGCAGGTC
OSH3.P2	GGATTCTATGATCTAAATAATATAACGTCTAATAGATATGAAAAAGACAAAGAAATAGTAAAATTTACCACAATTTAATCTCTGATATCATCGATGAATTCGAG
SAC1.P1	AATATAAACACTATTTTTTCCACTTTCTTTAATCTAACCTTATACGCAACTATACAATTATATAACAGAAAATGGTGTTAGAAGCTTCGTACGCTGCAGGTC
SAC1.P2	ATCTATTATATAAAATAAGCAGCTACAACTAAAGACAACTTTCTAAAAAAAAAAACAACCCCCACAGCTAATCAATTCTTTCTGATATCATCGATGAATTCGAG
DNF2.P5	GGCGCGCCATGACTAAAAATAAGCACAATTTCACGC
DNF2.P6	ATACGCGTTTAATTCATTGAAGATACTCTTTTTTG
DRS2.P1	TAACTAGTCTTTTAATATAGCCGAATTCCCCG
DRS2.P2	TATAGCGGCCGCGAGTTGGTTAATAACAAAATATCAG
OSH4.P3	GGAACTTTGAAAGACTCAAAGTATGACCATGGTGAAGCCAAGCATTGGAGAGTTAACTTGAAAAAGTTGGAAGATGAAAAAGAAATAGTCTTTGGTGCTGGCGCAGGTGCTTC
OSH4.P4	GTAATCCTTCTATAGTAAACTGTTTATATTTAAATGATGTACTACTATTATAAACATTATTTTACGAAATTGAAAAAACCTACTCTAAATTCATTTATCTGATATCATCGATGAATTCGAG
DRS2.P3	CAAGTTGAAGGTCAAGATCAAGATAAAATTGTTAGATTATATGATACTACTAAAAAAAGAGGAGTTTTTGGGGAATTATCAGAAAGTAAGGGTGCTGGCGCAGGTGCTTC
DRS2.P4	GGGAGTGAGATAGTTGTATATCAAACAGTTCTATAGCTTTAAATAAATAAAAAAAAAACATTCATTGATTGCATTAATATACTACTCATACTCTATTTATCTGATATCATCGATGAATTCGAG
DNF2.P7	GGTAGCTACAGAAGAAATTCCATTAGAAGATTTTGATGATGAACAAAAAAGAGCATCTAGAATAAGCTACGAAAATCAAAAAAGAGTATCTTCAATGAATGGTGCTGGCGCAGGTGCTTC
DNF2.P8	CCTCTCATTCTTTATATAAATATGCTTGAAATTCTTGTATGTGTGTTTGTTGTCTATAATGTTTTCTTTTATGTTATGCAAATGAAAATTGCTGTTATCTGATATCATCGATGAATTCGAG
MLC1.P1	GATGAGTTATTAAAAGGGGTCAATGTAACTTCTGATGGAAATGTGGATTATGTTGAATTTGTCAAATCAATTTTAGACCAAGGTGCTGGCGCAGGTGCTTC
MLC1.P2	CGAACAAGACTATACAATAACTATAATTTGTAAAACTTGTAGTATATATATTTCAATGGTTAATTGTAAATTTTCTTTTATTCTGATATCATCGATGAATTCGAG
CDC10.P1	CAATCAAACCAAGATTTGAAGAACACCTCTGGTGTGCCAAATGCTCCTATGTTCCAATCAACTACAGGTACTGCTGCTGCTAGAGGTGCTGGCGCAGGTGCTTC
CDC10.P2	CGCGTTTTGCTTTTCAACAAACACACAAAAGAAGAGGAATACAAAAAAGTAAAATCACATTATATCAATAACAAACCTGATATCATCGATGAATTCGAG
D4H.P1	ACGGCGCGCCGACTAGTGGATCCAAGGGAAAAATAAACTTAGATCATAGTGGAGCC
D4H.P2	GATACGCGTTAATTGTAAGTAATACTAGATCCAGGG
RT.PCR	
DRS2.pTm	CGGCATTAGTGGTTACCATGT
DRS2.mTm	GCAGGATACCAACCTAACCATAA
DNF1.pTm	GCACAATCAACGGGAAGTCATAC
DNF1.mTm	AATGCCTGCACGTTTATCCAA
DNF2.pTm	TGACAAGACCGGGACATTA
DNF2.mTm	TCCGTAACCCAGCCAAT
DNF3.pTm	AAGCATCAATGGCAGGTCATC
DNF3.mTm	GCTGCCGTGCTTGTTCTTG
OSH4.pTm	TTTGATTACTGCTGCTCCTT
OSH4.mTm	AATGTGACCACTGGATGCTT
OSH7a.pTm	TGAAGCAGCTGTCAAATCTAATGTG
OSH7a.mTm	CTGTCCCTCGTTATCCATTTCATC
OSH7α.pTm	GTAACTCGTCTGCAGCAATCATG
OSH7 α.mTm	CCTCGTTGTCCCATTTACCAA
OSH2.pTm	AAGCCAGAAAACAGAGGGAAGAT
OSH2.mTm	TCACTGGATGCTTTCTCTTAACAAA
OSH3.pTm	GGGTAAACTTGCACCTACGGATT
OSH3.mTm	GCAGTGTCTGTATCTCCCTTTTCA
UME6.pTm	TGGCTCCACTTACAAATCATAGTGA
UME6.mTm	GCTTTACCAATCCTAGTCCCAACTC

(*Continued*)

Table 2. (Continued)

PRIMER	SEQUENCE
SAC1.pTm	CCCATTCCACAGCAACAGATG
SAC1.mTm	TTCAACACCACCTCCCAGTGT
ACT1.pTm	ATGTTCCCAGGTATTGCTGA
ACT1.mTm	ACATTTGTGGTGAACAATGG
TDH3.pTm	ATCCCACAAGGACTGGAGA
TDH3.mTm	GCAGAAGCTTTAGCAACGTG

https://doi.org/10.1371/journal.pgen.1010549.t002

into plasmid *pExp-pACT1-mScarlet-CtRac1* [92], using AscI and MluI unique restriction sites, yielding *pExp-pACT1-mScarlet-D4H*. This plasmid was linearized with NcoI and integrated into the *RP10* locus. All other pExp plasmids were linearized with StuI and integrated into the *RP10* locus. pDUP3 and pDUP5 plasmids were digested with NgoMIV to release the cassette to be integrated into the *NEUTL5* locus.

Two independent clones of each strain were generated and confirmed by PCR. RT-PCR was also performed, where relevant, using the primers (GENE.pTm and GENE.mTm) listed in Table 2 or previously described [93] and RNA extraction was carried out using Master Pure yeast RNA extraction purification kit (Epicentre). All PCR amplified products were confirmed by sequencing (Eurofins MWG Operon, Ebersberg, Germany).

Microscopy analyses

Colony and cell morphology imaging were performed as described [83]. Briefly, plates were incubated for 3–6 days prior to imaging with a Leica MZ6 binocular (x20) and cells (budding or serum-induced) were imaged by differential interference contrast with a microscope Leica DMR, using an ImagingSource DMK 23UX174 sCMOS camera.

Time lapses and fluorescent images were obtained using a spinning disk confocal microscope (inverted IX81 Olympus microscope with a 100X objective and a numerical aperture 1.45) and an EMCCD camera (Andor technology, UK). Z-stacks (images of 0.4 μm sections) were acquired every 5 min, as described [56]. Maximum or sum intensity projections were generated from 21 z-sections with ImageJ software. Laser illuminations of 445 nm (Turquoise), 488 nm (GFP), 561 nm (mScarlet) and 640 nm (iRFP) were used. CRIBGFP distribution experiments were carried out as described [48]. For filipin analyses, widefield images were acquired on an inverted ZEISS Axio Observer Z1 microscope with a 100X (1.3 NA) objective. Huygens professional software version 18.04 (Scientific-Volume Imaging) was used to deconvolve z-stack images of cells expressing PH-FAPP1$^{[E50A,H54A]}$-GFP. Bars are 5 μm.

Filament lengths and diameters were measured from DIC images, using ImageJ. Golgi cisternae were quantitated from deconvolved MAX projection images. Quantitation of PI(4)P distribution was performed on SUM projections, using the Matlab program HyphalPolarity [56]. Quantitation of PS PM and internal mean signals was performed on central z-sections, also using the Matlab program HyphalPolarity. Central Z sections are middle planes of the cells. Unless indicated otherwise, error bars represent the standard deviations. Statistical significance was determined with Student's unpaired two-tailed *t* test.

Virulence assays

HDC was induced in 10 Balb/C mice (Charles Rivers, Italy) per group by injecting the lateral tail vein with an inoculum of 5 x 10^5 cells [94]. Animal body weight was monitored daily and

animals were sacrificed by cervical dislocation when they had lost more than 20% of their weight.

Supporting information

S1 Fig. Flippase deletion mutant strains verification. A) *DRS2* and *DNF1-3* transcript levels. mRNA and cDNA were prepared from the indicated strains, as in Fig 1A. *DRS2* and *DNF1-3* transcripts were determined by RT-PCR, using *DRS2*.pTm/*DRS2*.mTm (62 bp), *DNF1*.pTm/*DNF1*.mTm (73 bp), *DNF2*.pTm/*DNF2*.mTm (106 bp) and *DNF3*.pTm/*DNF3*.mTm (104 bp) primer pairs, respectively. Actin (*ACT1*) transcript levels (*ACT1*.pTm/*ACT1*.mTm primer pair) were used for normalization. B) *OSH4 and OSH7* transcript levels. mRNA and cDNA were prepared from the indicated strains, as in Fig 8A. Transcripts were determined as in S1A Fig, using *OSH4*.pTm/*OSH4*.mTm (69 bp), *OSH7A*.pTm/*OSH7A*.mTm (84 bp), *OSH7*α.pTm/*OSH7*α.mTm (65 bp) primer pairs, respectively. C) Deletion of *DRS2* does not result in a significant alteration of *OSH4* expression. mRNA and cDNA were prepared from the indicated strains grown without (0) or with serum for 120 min (120). *OSH4* and *DRS2* transcripts were determined by qRT-PCR using primer pairs *OSH4*.pTm/*OSH4*.mTm and *DRS2*.pTm/*DRS2*.mTm as above. Bars indicate the mean ± SD of 2 biological samples ($n = 3$ determinations each). *ACT1* transcript levels were used for normalization.
(TIF)

S2 Fig. Deletion of *OSH2* and *OSH3* do not recover invasive filamentous growth in the *drs2* mutant. A) *DRS2* and *OSH2-3* transcript levels. mRNA and cDNA were prepared from the indicated strains, and transcripts were determined as in S1A Fig, using *OSH2*.pTm/*OSH2*.mTm (74 bp), *OSH3*.pTm/*OSH3*.mTm (74 bp) primer pairs, respectively. B) Invasive growth is not restored in the *drs2* mutant upon deletion of *OSH2* or *OSH3*. The indicated strains, WT (PY4861), *osh2/osh2* (*osh2*, PY3977), *osh3/osh3* (*osh3*, PY4002), *drs2/drs2* (*drs2*, PY3375), *drs2/drs2 osh2/osh2* (*drs2 osh2*, PY6408) and *drs2/drs2 osh3/osh3* (*drs2 osh3*, PY6431), were grown on agar-containing serum media and images were taken after 6 days. Similar results were observed in 2 independent experiments. C) Hyphal growth is not restored in the *drs2* mutant upon deletion of *OSH2* or *OSH3*. At 90 min, the percent of filamentous cells, was determined from 3 independent biological samples for the WT, *drs2*, *osh2*, *osh3*, *drs2 osh2* and *drs2 osh3* strains; $n \sim 100$ cells.
(TIF)

S1 Movie. Active Cdc42 and Mlc1 distribution during filament extension in wild-type cells. Time lapse of wild-type (PY6450) cells expressing Mlc1-mScarlet, together with CRIB-GFP incubated in the presence of serum. Images were taken every 10 min and maximum projections of 21 z-sections are shown.
(AVI)

S2 Movie. Active Cdc42 delocalizes prior to Mlc1 upon filament extension in the *drs2* mutant. Time lapse of *drs2/drs2* cells (PY6389) expressing Mlc1-mScarlet, together with CRIB-GFP incubated in the presence of serum. Images were taken every 10 min and maximum projections of 21 z-sections are shown.
(AVI)

Acknowledgments

We thank J. Berman, S. Martin, A. Mitchell, J.C. Shieh and J. Wendland, for plasmids and strains. We thank the Platform Resources in Imaging and Scientific Microscopy facility

(PRISM; M. Mondin, S. Lachambre, and B. Monterroso), and Microscopy Imaging Côte d'Azur (MICA) for microscopy support.

Author Contributions

Conceptualization: Martine Bassilana.

Formal analysis: Miguel A. Basante-Bedoya, Martine Bassilana.

Funding acquisition: Rocio Garcia-Rodas, Oscar Zaragoza, Robert A. Arkowitz, Martine Bassilana.

Investigation: Miguel A. Basante-Bedoya, Stéphanie Bogliolo, Rocio Garcia-Rodas.

Methodology: Miguel A. Basante-Bedoya.

Project administration: Robert A. Arkowitz, Martine Bassilana.

Resources: Robert A. Arkowitz.

Supervision: Martine Bassilana.

Visualization: Robert A. Arkowitz.

Writing – original draft: Martine Bassilana.

Writing – review & editing: Oscar Zaragoza, Robert A. Arkowitz, Martine Bassilana.

References

1. Das A, Slaughter BD, Unruh JR, Bradford WD, Alexander R, Rubinstein B, et al. Flippase-mediated phospholipid asymmetry promotes fast Cdc42 recycling in dynamic maintenance of cell polarity. Nat Cell Biol. 2012; 14(3):304–10. Epub 2012/02/22. https://doi.org/10.1038/ncb2444 PMID: 22344035; PubMed Central PMCID: PMC3534761.
2. Fairn GD, Hermansson M, Somerharju P, Grinstein S. Phosphatidylserine is polarized and required for proper Cdc42 localization and for development of cell polarity. Nat Cell Biol. 2011; 13(12):1424–30. Epub 2011/10/04. https://doi.org/10.1038/ncb2351 PMID: 21964439.
3. Meca J, Massoni-Laporte A, Martinez D, Sartorel E, Loquet A, Habenstein B, et al. Avidity-driven polarity establishment via multivalent lipid-GTPase module interactions. EMBO J. 2019; 38(3). Epub 2018/12/19. https://doi.org/10.15252/embj.201899652 PMID: 30559330; PubMed Central PMCID: PMC6356062.
4. Haupt A, Minc N. Gradients of phosphatidylserine contribute to plasma membrane charge localization and cell polarity in fission yeast. Mol Biol Cell. 2017; 28(1):210–20. Epub 2016/11/18. https://doi.org/10.1091/mbc.E16-06-0353 PMID: 27852900; PubMed Central PMCID: PMC5221626.
5. Kay JG, Fairn GD. Distribution, dynamics and functional roles of phosphatidylserine within the cell. Cell Commun Signal. 2019; 17(1):126. Epub 2019/10/17. https://doi.org/10.1186/s12964-019-0438-z PMID: 31615534; PubMed Central PMCID: PMC6792266.
6. Noack LC, Jaillais Y. Functions of Anionic Lipids in Plants. Annu Rev Plant Biol. 2020; 71:71–102. Epub 2020/05/23. https://doi.org/10.1146/annurev-arplant-081519-035910 PMID: 32442391.
7. Cassilly CD, Reynolds TB. PS, It's Complicated: The Roles of Phosphatidylserine and Phosphatidylethanolamine in the Pathogenesis of Candida albicans and Other Microbial Pathogens. J Fungi (Basel). 2018; 4(1). Epub 2018/02/21. https://doi.org/10.3390/jof4010028 PMID: 29461490; PubMed Central PMCID: PMC5872331.
8. Rizzo J, Stanchev LD, da Silva VKA, Nimrichter L, Pomorski TG, Rodrigues ML. Role of lipid transporters in fungal physiology and pathogenicity. Comput Struct Biotechnol J. 2019; 17:1278–89. Epub 2020/01/11. https://doi.org/10.1016/j.csbj.2019.09.001 PMID: 31921394; PubMed Central PMCID: PMC6944739.
9. Chen YL, Montedonico AE, Kauffman S, Dunlap JR, Menn FM, Reynolds TB. Phosphatidylserine synthase and phosphatidylserine decarboxylase are essential for cell wall integrity and virulence in Candida albicans. Mol Microbiol. 2010; 75(5):1112–32. Epub 2010/02/06. https://doi.org/10.1111/j.1365-2958.2009.07018.x PMID: 20132453.

10. Chen T, Jackson JW, Tams RN, Davis SE, Sparer TE, Reynolds TB. Exposure of Candida albicans beta (1,3)-glucan is promoted by activation of the Cek1 pathway. PLoS Genet. 2019; 15(1):e1007892. Epub 2019/02/01. https://doi.org/10.1371/journal.pgen.1007892 PMID: 30703081; PubMed Central PMCID: PMC6372213.

11. Lenoir G, D'Ambrosio JM, Dieudonne T, Copic A. Transport Pathways That Contribute to the Cellular Distribution of Phosphatidylserine. Front Cell Dev Biol. 2021; 9:737907. Epub 2021/09/21. https://doi.org/10.3389/fcell.2021.737907 PMID: 34540851; PubMed Central PMCID: PMC8440936.

12. Lyons JA, Timcenko M, Dieudonne T, Lenoir G, Nissen P. P4-ATPases: how an old dog learnt new tricks—structure and mechanism of lipid flippases. Curr Opin Struct Biol. 2020; 63:65–73. Epub 2020/06/04. https://doi.org/10.1016/j.sbi.2020.04.001 PMID: 32492637.

13. Lopez-Marques RL. Lipid flippases in polarized growth. Curr Genet. 2021; 67(2):255–62. Epub 2021/01/04. https://doi.org/10.1007/s00294-020-01145-0 PMID: 33388852.

14. Lenoir G, Williamson P, Puts CF, Holthuis JC. Cdc50p plays a vital role in the ATPase reaction cycle of the putative aminophospholipid transporter Drs2p. J Biol Chem. 2009; 284(27):17956–67. Epub 2009/05/05. https://doi.org/10.1074/jbc.M109.013722 PMID: 19411703; PubMed Central PMCID: PMC2709398.

15. Saito K, Fujimura-Kamada K, Furuta N, Kato U, Umeda M, Tanaka K. Cdc50p, a protein required for polarized growth, associates with the Drs2p P-type ATPase implicated in phospholipid translocation in Saccharomyces cerevisiae. Mol Biol Cell. 2004; 15(7):3418–32. Epub 2004/04/20. https://doi.org/10.1091/mbc.e03-11-0829 PMID: 15090616; PubMed Central PMCID: PMC452594.

16. Timcenko M, Lyons JA, Januliene D, Ulstrup JJ, Dieudonne T, Montigny C, et al. Structure and autoregulation of a P4-ATPase lipid flippase. Nature. 2019; 571(7765):366–70. Epub 2019/06/28. https://doi.org/10.1038/s41586-019-1344-7 PMID: 31243363.

17. Natarajan P, Wang J, Hua Z, Graham TR. Drs2p-coupled aminophospholipid translocase activity in yeast Golgi membranes and relationship to in vivo function. Proc Natl Acad Sci U S A. 2004; 101(29):10614–9. Epub 2004/07/14. https://doi.org/10.1073/pnas.0404146101 PMID: 15249668; PubMed Central PMCID: PMC489982.

18. Zhou X, Graham TR. Reconstitution of phospholipid translocase activity with purified Drs2p, a type-IV P-type ATPase from budding yeast. Proc Natl Acad Sci U S A. 2009; 106(39):16586–91. Epub 2009/10/07. https://doi.org/10.1073/pnas.0904293106 PMID: 19805341; PubMed Central PMCID: PMC2757829.

19. Best JT, Xu P, Graham TR. Phospholipid flippases in membrane remodeling and transport carrier biogenesis. Curr Opin Cell Biol. 2019; 59:8–15. Epub 2019/03/22. https://doi.org/10.1016/j.ceb.2019.02.004 PMID: 30897446; PubMed Central PMCID: PMC6726550.

20. Hua Z, Fatheddin P, Graham TR. An essential subfamily of Drs2p-related P-type ATPases is required for protein trafficking between Golgi complex and endosomal/vacuolar system. Mol Biol Cell. 2002; 13(9):3162–77. Epub 2002/09/11. https://doi.org/10.1091/mbc.e02-03-0172 PMID: 12221123; PubMed Central PMCID: PMC124150.

21. Chen CY, Ingram MF, Rosal PH, Graham TR. Role for Drs2p, a P-type ATPase and potential aminophospholipid translocase, in yeast late Golgi function. J Cell Biol. 1999; 147(6):1223–36. Epub 1999/12/22. https://doi.org/10.1083/jcb.147.6.1223 PMID: 10601336; PubMed Central PMCID: PMC2168089.

22. Pomorski T, Lombardi R, Riezman H, Devaux PF, van Meer G, Holthuis JC. Drs2p-related P-type ATPases Dnf1p and Dnf2p are required for phospholipid translocation across the yeast plasma membrane and serve a role in endocytosis. Mol Biol Cell. 2003; 14(3):1240–54. Epub 2003/03/13. https://doi.org/10.1091/mbc.e02-08-0501 PMID: 12631737; PubMed Central PMCID: PMC151593.

23. Frosig MM, Costa SR, Liesche J, Osterberg JT, Hanisch S, Nintemann S, et al. Pseudohyphal growth in Saccharomyces cerevisiae involves protein kinase-regulated lipid flippases. J Cell Sci. 2020; 133(15). Epub 2020/07/15. https://doi.org/10.1242/jcs.235994 PMID: 32661085.

24. Sartorel E, Barrey E, Lau RK, Thorner J. Plasma membrane aminoglycerolipid flippase function is required for signaling competence in the yeast mating pheromone response pathway. Mol Biol Cell. 2015; 26(1):134–50. Epub 2014/11/08. https://doi.org/10.1091/mbc.E14-07-1193 PMID: 25378585; PubMed Central PMCID: PMC4279224.

25. Schultzhaus Z, Yan H, Shaw BD. Aspergillus nidulans flippase DnfA is cargo of the endocytic collar and plays complementary roles in growth and phosphatidylserine asymmetry with another flippase, DnfB. Mol Microbiol. 2015; 97(1):18–32. Epub 2015/04/08. https://doi.org/10.1111/mmi.13019 PMID: 25846564.

26. Yun Y, Guo P, Zhang J, You H, Guo P, Deng H, et al. Flippases play specific but distinct roles in the development, pathogenicity, and secondary metabolism of Fusarium graminearum. Mol Plant Pathol. 2020; 21(10):1307–21. Epub 2020/09/04. https://doi.org/10.1111/mpp.12985 PMID: 32881238; PubMed Central PMCID: PMC7488471.

27. Wong LH, Gatta AT, Levine TP. Lipid transfer proteins: the lipid commute via shuttles, bridges and tubes. Nat Rev Mol Cell Biol. 2019; 20(2):85–101. Epub 2018/10/20. https://doi.org/10.1038/s41580-018-0071-5 PMID: 30337668.

28. Maeda K, Anand K, Chiapparino A, Kumar A, Poletto M, Kaksonen M, et al. Interactome map uncovers phosphatidylserine transport by oxysterol-binding proteins. Nature. 2013; 501(7466):257–61. Epub 2013/08/13. https://doi.org/10.1038/nature12430 PMID: 23934110.

29. Moser von Filseck J, Vanni S, Mesmin B, Antonny B, Drin G. A phosphatidylinositol-4-phosphate powered exchange mechanism to create a lipid gradient between membranes. Nat Commun. 2015; 6:6671. Epub 2015/04/08. https://doi.org/10.1038/ncomms7671 PMID: 25849868.

30. de Saint-Jean M, Delfosse V, Douguet D, Chicanne G, Payrastre B, Bourguet W, et al. Osh4p exchanges sterols for phosphatidylinositol 4-phosphate between lipid bilayers. J Cell Biol. 2011; 195 (6):965–78. Epub 2011/12/14. https://doi.org/10.1083/jcb.201104062 PMID: 22162133; PubMed Central PMCID: PMC3241724.

31. Muthusamy BP, Raychaudhuri S, Natarajan P, Abe F, Liu K, Prinz WA, et al. Control of protein and sterol trafficking by antagonistic activities of a type IV P-type ATPase and oxysterol binding protein homologue. Mol Biol Cell. 2009; 20(12):2920–31. Epub 2009/05/01. https://doi.org/10.1091/mbc.e08-10-1036 PMID: 19403696; PubMed Central PMCID: PMC2695799.

32. Gilbert MJ, Thornton CR, Wakley GE, Talbot NJ. A P-type ATPase required for rice blast disease and induction of host resistance. Nature. 2006; 440(7083):535–9. Epub 2006/03/24. https://doi.org/10.1038/nature04567 PMID: 16554820.

33. Li B, Dong X, Zhao R, Kou R, Zheng X, Zhang H. The t-SNARE protein FgPep12, associated with FgVam7, is essential for ascospore discharge and plant infection by trafficking Ca2+ ATPase FgNeo1 between Golgi and endosome/vacuole in Fusarium graminearum. PLoS Pathog. 2019; 15(5): e1007754. Epub 2019/05/09. https://doi.org/10.1371/journal.ppat.1007754 PMID: 31067272; PubMed Central PMCID: PMC6527245.

34. Zhang J, Yun Y, Lou Y, Abubakar YS, Guo P, Wang S, et al. FgAP-2 complex is essential for pathogenicity and polarised growth and regulates the apical localisation of membrane lipid flippases in Fusarium graminearum. Cell Microbiol. 2019; 21(8):e13041. Epub 2019/05/16. https://doi.org/10.1111/cmi.13041 PMID: 31087807.

35. Douglas LM, Konopka JB. Plasma membrane architecture protects Candida albicans from killing by copper. PLoS Genet. 2019; 15(1):e1007911. Epub 2019/01/12. https://doi.org/10.1371/journal.pgen.1007911 PMID: 30633741; PubMed Central PMCID: PMC6345494.

36. Labbaoui H, Bogliolo S, Ghugtyal V, Solis NV, Filler SG, Arkowitz RA, et al. Role of Arf GTPases in fungal morphogenesis and virulence. PLoS Pathog. 2017; 13(2):e1006205. Epub 2017/02/14. https://doi.org/10.1371/journal.ppat.1006205 PMID: 28192532; PubMed Central PMCID: PMC5325608.

37. Xu D, Zhang X, Zhang B, Zeng X, Mao H, Xu H, et al. The lipid flippase subunit Cdc50 is required for antifungal drug resistance, endocytosis, hyphal development and virulence in Candida albicans. FEMS Yeast Res. 2019; 19(3). Epub 2019/04/21. https://doi.org/10.1093/femsyr/foz033 PMID: 31004489.

38. Jain BKW A. S.; Reynolds T. B.; Graham T. R. Lipid transport by Candida albicans Dnf2 is required for hyphal growth and virulence. bioRxiv. 2022: https://doi.org/10.1101/2022.06.10.495726

39. Prasad R, De Wergifosse P, Goffeau A, Balzi E. Molecular cloning and characterization of a novel gene of Candida albicans, CDR1, conferring multiple resistance to drugs and antifungals. Curr Genet. 1995; 27(4):320–9. Epub 1995/03/01. https://doi.org/10.1007/BF00352101 PMID: 7614555.

40. Carlisle PL, Kadosh D. Candida albicans Ume6, a filament-specific transcriptional regulator, directs hyphal growth via a pathway involving Hgc1 cyclin-related protein. Eukaryot Cell. 2010; 9(9):1320–8. Epub 2010/07/27. https://doi.org/10.1128/EC.00046-10 PMID: 20656912; PubMed Central PMCID: PMC2937344.

41. Banerjee M, Thompson DS, Lazzell A, Carlisle PL, Pierce C, Monteagudo C, et al. UME6, a novel filament-specific regulator of Candida albicans hyphal extension and virulence. Mol Biol Cell. 2008; 19 (4):1354–65. Epub 2008/01/25. https://doi.org/10.1091/mbc.e07-11-1110 PMID: 18216277; PubMed Central PMCID: PMC2291399.

42. Zheng X, Wang Y, Wang Y. Hgc1, a novel hypha-specific G1 cyclin-related protein regulates Candida albicans hyphal morphogenesis. EMBO J. 2004; 23(8):1845–56. Epub 2004/04/09. https://doi.org/10.1038/sj.emboj.7600195 PMID: 15071502; PubMed Central PMCID: PMC394249.

43. Naglik JR, Gaffen SL, Hube B. Candidalysin: discovery and function in Candida albicans infections. Curr Opin Microbiol. 2019; 52:100–9. Epub 2019/07/10. https://doi.org/10.1016/j.mib.2019.06.002 PMID: 31288097; PubMed Central PMCID: PMC6687503.

44. Tsuchimori N, Sharkey LL, Fonzi WA, French SW, Edwards JE Jr., Filler SG. Reduced virulence of HWP1-deficient mutants of Candida albicans and their interactions with host cells. Infect Immun. 2000;

68(4):1997–2002. Epub 2000/03/18. https://doi.org/10.1128/IAI.68.4.1997-2002.2000 PMID: 10722594; PubMed Central PMCID: PMC97378.

45. Cleary IA, Reinhard SM, Miller CL, Murdoch C, Thornhill MH, Lazzell AL, et al. Candida albicans adhesin Als3p is dispensable for virulence in the mouse model of disseminated candidiasis. Microbiology (Reading). 2011; 157(Pt 6):1806–15. Epub 2011/03/26. https://doi.org/10.1099/mic.0.046326-0 PMID: 21436220; PubMed Central PMCID: PMC3167918.

46. Hube B, Monod M, Schofield DA, Brown AJ, Gow NA. Expression of seven members of the gene family encoding secretory aspartyl proteinases in Candida albicans. Mol Microbiol. 1994; 14(1):87–99. Epub 1994/10/01. https://doi.org/10.1111/j.1365-2958.1994.tb01269.x PMID: 7830564.

47. Gonzalez-Novo A, Jimenez J, Garcia MJ, Rios-Serrano I, Pla J, Jimenez A, et al. Dynamics of CaCdc10, a septin of Candida albicans, in living cells and during infection. Int Microbiol. 2004; 7 (2):105–12. Epub 2004/07/13. PMID: 15248158.

48. Corvest V, Bogliolo S, Follette P, Arkowitz RA, Bassilana M. Spatiotemporal regulation of Rho1 and Cdc42 activity during Candida albicans filamentous growth. Mol Microbiol. 2013; 89(4):626–48. Epub 2013/06/26. https://doi.org/10.1111/mmi.12302 PMID: 23796158.

49. Crampin H, Finley K, Gerami-Nejad M, Court H, Gale C, Berman J, et al. Candida albicans hyphae have a Spitzenkorper that is distinct from the polarisome found in yeast and pseudohyphae. J Cell Sci. 2005; 118(Pt 13):2935–47. Epub 2005/06/25. https://doi.org/10.1242/jcs.02414 PMID: 15976451.

50. Puerner C, Serrano A, Wakade RS, Bassilana M, Arkowitz RA. A Myosin Light Chain Is Critical for Fungal Growth Robustness in Candida albicans. mBio. 2021; 12(5):e0252821. Epub 2021/10/06. https://doi.org/10.1128/mBio.02528-21 PMID: 34607458.

51. Vauchelles R, Stalder D, Botton T, Arkowitz RA, Bassilana M. Rac1 dynamics in the human opportunistic fungal pathogen Candida albicans. PLoS One. 2010; 5(10):e15400. Epub 2010/11/10. https://doi.org/10.1371/journal.pone.0015400 PMID: 21060846; PubMed Central PMCID: PMC2965673.

52. Weiner A, Orange F, Lacas-Gervais S, Rechav K, Ghugtyal V, Bassilana M, et al. On-site secretory vesicle delivery drives filamentous growth in the fungal pathogen Candida albicans. Cell Microbiol. 2019; 21(1):e12963. Epub 2018/10/16. https://doi.org/10.1111/cmi.12963 PMID: 30321912.

53. Del Vecchio K, Stahelin RV. Investigation of the phosphatidylserine binding properties of the lipid biosensor, Lactadherin C2 (LactC2), in different membrane environments. J Bioenerg Biomembr. 2018; 50 (1):1–10. Epub 2018/02/11. https://doi.org/10.1007/s10863-018-9745-0 PMID: 29426977; PubMed Central PMCID: PMC5820145.

54. Leventis PA, Grinstein S. The distribution and function of phosphatidylserine in cellular membranes. Annu Rev Biophys. 2010; 39:407–27. Epub 2010/03/03. https://doi.org/10.1146/annurev.biophys.093008.131234 PMID: 20192774.

55. Yeung T, Gilbert GE, Shi J, Silvius J, Kapus A, Grinstein S. Membrane phosphatidylserine regulates surface charge and protein localization. Science. 2008; 319(5860):210–3. Epub 2008/01/12. https://doi.org/10.1126/science.1152066 PMID: 18187657.

56. Ghugtyal V, Garcia-Rodas R, Seminara A, Schaub S, Bassilana M, Arkowitz RA. Phosphatidylinositol-4-phosphate-dependent membrane traffic is critical for fungal filamentous growth. Proc Natl Acad Sci U S A. 2015; 112(28):8644–9. Epub 2015/07/01. https://doi.org/10.1073/pnas.1504259112 PMID: 26124136; PubMed Central PMCID: PMC4507248.

57. Vernay A, Schaub S, Guillas I, Bassilana M, Arkowitz RA. A steep phosphoinositide bis-phosphate gradient forms during fungal filamentous growth. J Cell Biol. 2012; 198(4):711–30. Epub 2012/08/15. https://doi.org/10.1083/jcb.201203099 PMID: 22891265; PubMed Central PMCID: PMC3514036.

58. Martin SW, Konopka JB. Lipid raft polarization contributes to hyphal growth in Candida albicans. Eukaryot Cell. 2004; 3(3):675–84. Epub 2004/06/11. https://doi.org/10.1128/EC.3.3.675-684.2004 PMID: 15189988; PubMed Central PMCID: PMC420133.

59. Kishimoto T, Mioka T, Itoh E, Williams DE, Andersen RJ, Tanaka K. Phospholipid flippases and Sfk1 are essential for the retention of ergosterol in the plasma membrane. Mol Biol Cell. 2021; 32(15):1374–92. Epub 2021/05/27. https://doi.org/10.1091/mbc.E20-11-0699 PMID: 34038161.

60. Koselny K, Mutlu N, Minard AY, Kumar A, Krysan DJ, Wellington M. A Genome-Wide Screen of Deletion Mutants in the Filamentous Saccharomyces cerevisiae Background Identifies Ergosterol as a Direct Trigger of Macrophage Pyroptosis. mBio. 2018; 9(4). Epub 2018/08/02. https://doi.org/10.1128/mBio.01204-18 PMID: 30065091; PubMed Central PMCID: PMC6069111.

61. Maekawa M, Yang Y, Fairn GD. Perfringolysin O Theta Toxin as a Tool to Monitor the Distribution and Inhomogeneity of Cholesterol in Cellular Membranes. Toxins (Basel). 2016; 8(3). Epub 2016/03/24. https://doi.org/10.3390/toxins8030067 PMID: 27005662; PubMed Central PMCID: PMC4810212.

62. Marek M, Vincenzetti V, Martin SG. Sterol biosensor reveals LAM-family Ltc1-dependent sterol flow to endosomes upon Arp2/3 inhibition. J Cell Biol. 2020; 219(6). Epub 2020/04/23. https://doi.org/10.1083/jcb.202001147 PMID: 32320462; PubMed Central PMCID: PMC7265315.

63. Hur HS, Ryu JH, Kim KH, Kim J. Characterization of Osh3, an oxysterol-binding protein, in filamentous growth of Saccharomyces cerevisiae and Candida albicans. J Microbiol. 2006; 44(5):523–9. Epub 2006/11/04. PMID: 17082746.

64. Stefan CJ, Manford AG, Baird D, Yamada-Hanff J, Mao Y, Emr SD. Osh proteins regulate phosphoinositide metabolism at ER-plasma membrane contact sites. Cell. 2011; 144(3):389–401. Epub 2011/02/08. https://doi.org/10.1016/j.cell.2010.12.034 PMID: 21295699.

65. Zewe JP, Wills RC, Sangappa S, Goulden BD, Hammond GR. SAC1 degrades its lipid substrate PtdIns4P in the endoplasmic reticulum to maintain a steep chemical gradient with donor membranes. Elife. 2018; 7. Epub 2018/02/21. https://doi.org/10.7554/eLife.35588 PMID: 29461204; PubMed Central PMCID: PMC5829913.

66. Zhang B, Yu Q, Jia C, Wang Y, Xiao C, Dong Y, et al. The actin-related protein Sac1 is required for morphogenesis and cell wall integrity in Candida albicans. Fungal Genet Biol. 2015; 81:261–70. Epub 2015/01/13. https://doi.org/10.1016/j.fgb.2014.12.007 PMID: 25575432.

67. Quon E, Sere YY, Chauhan N, Johansen J, Sullivan DP, Dittman JS, et al. Endoplasmic reticulum-plasma membrane contact sites integrate sterol and phospholipid regulation. PLoS Biol. 2018; 16(5): e2003864. Epub 2018/05/22. https://doi.org/10.1371/journal.pbio.2003864 PMID: 29782498; PubMed Central PMCID: PMC5983861.

68. Parsons AB, Lopez A, Givoni IE, Williams DE, Gray CA, Porter J, et al. Exploring the mode-of-action of bioactive compounds by chemical-genetic profiling in yeast. Cell. 2006; 126(3):611–25. Epub 2006/08/12. https://doi.org/10.1016/j.cell.2006.06.040 PMID: 16901791.

69. Cassilly CD, Maddox MM, Cherian PT, Bowling JJ, Hamann MT, Lee RE, et al. SB-224289 Antagonizes the Antifungal Mechanism of the Marine Depsipeptide Papuamide A. PLoS One. 2016; 11(5): e0154932. Epub 2016/05/18. https://doi.org/10.1371/journal.pone.0154932 PMID: 27183222; PubMed Central PMCID: PMC4868317.

70. Ling Y, Hayano S, Novick P. Osh4p is needed to reduce the level of phosphatidylinositol-4-phosphate on secretory vesicles as they mature. Mol Biol Cell. 2014; 25(21):3389–400. Epub 2014/08/29. https://doi.org/10.1091/mbc.E14-06-1087 PMID: 25165144; PubMed Central PMCID: PMC4214785.

71. Buhler N, Hagiwara D, Takeshita N. Functional Analysis of Sterol Transporter Orthologues in the Filamentous Fungus Aspergillus nidulans. Eukaryot Cell. 2015; 14(9):908–21. Epub 2015/06/28. https://doi.org/10.1128/EC.00027-15 PMID: 26116213; PubMed Central PMCID: PMC4551590.

72. Hernandez-Gonzalez M, Bravo-Plaza I, Pinar M, de Los Rios V, Arst HN Jr., Penalva MA. Endocytic recycling via the TGN underlies the polarized hyphal mode of life. PLoS Genet. 2018; 14(4):e1007291. Epub 2018/04/03. https://doi.org/10.1371/journal.pgen.1007291 PMID: 29608571; PubMed Central PMCID: PMC5880334.

73. Schultzhaus Z, Cunningham GA, Mourino-Perez RR, Shaw BD. The phospholipid flippase DnfD localizes to late Golgi and is involved in asexual differentiation in Aspergillus nidulans. Mycologia. 2019; 111 (1):13–25. Epub 2019/01/31. https://doi.org/10.1080/00275514.2018.1543927 PMID: 30699058.

74. Bagnat M, Simons K. Cell surface polarization during yeast mating. Proc Natl Acad Sci U S A. 2002; 99 (22):14183–8. Epub 2002/10/11. https://doi.org/10.1073/pnas.172517799 PMID: 12374868; PubMed Central PMCID: PMC137858.

75. Wachtler V, Rajagopalan S, Balasubramanian MK. Sterol-rich plasma membrane domains in the fission yeast Schizosaccharomyces pombe. J Cell Sci. 2003; 116(Pt 5):867–74. Epub 2003/02/07. https://doi.org/10.1242/jcs.00299 PMID: 12571284.

76. Takeshita N, Higashitsuji Y, Konzack S, Fischer R. Apical sterol-rich membranes are essential for localizing cell end markers that determine growth directionality in the filamentous fungus Aspergillus nidulans. Mol Biol Cell. 2008; 19(1):339–51. Epub 2007/11/16. https://doi.org/10.1091/mbc.e07-06-0523 PMID: 18003978; PubMed Central PMCID: PMC2174190.

77. Hankins HM, Sere YY, Diab NS, Menon AK, Graham TR. Phosphatidylserine translocation at the yeast trans-Golgi network regulates protein sorting into exocytic vesicles. Mol Biol Cell. 2015; 26(25):4674–85. Epub 2015/10/16. https://doi.org/10.1091/mbc.E15-07-0487 PMID: 26466678; PubMed Central PMCID: PMC4678023.

78. Garcia-Rodas R, Labbaoui H, Orange F, Solis N, Zaragoza O, Filler SG, et al. Plasma Membrane Phosphatidylinositol-4-Phosphate Is Not Necessary for Candida albicans Viability yet Is Key for Cell Wall Integrity and Systemic Infection. mBio. 2022:e0387321. Epub 2022/02/16. https://doi.org/10.1128/mbio.03873-21 PMID: 35164565; PubMed Central PMCID: PMC8942462.

79. Stefan CJ, Trimble WS, Grinstein S, Drin G, Reinisch K, De Camilli P, et al. Membrane dynamics and organelle biogenesis-lipid pipelines and vesicular carriers. BMC Biol. 2017; 15(1):102. Epub 2017/11/02. https://doi.org/10.1186/s12915-017-0432-0 PMID: 29089042; PubMed Central PMCID: PMC5663033.

80. Xu P, Baldridge RD, Chi RJ, Burd CG, Graham TR. Phosphatidylserine flipping enhances membrane curvature and negative charge required for vesicular transport. J Cell Biol. 2013; 202(6):875–86. Epub 2013/09/11. https://doi.org/10.1083/jcb.201305094 PMID: 24019533; PubMed Central PMCID: PMC3776346.

81. Berkow EL, Lockhart SR. Fluconazole resistance in Candida species: a current perspective. Infect Drug Resist. 2017; 10:237–45. Epub 2017/08/18. https://doi.org/10.2147/IDR.S118892 PMID: 28814889; PubMed Central PMCID: PMC5546770.

82. Shen XX, Opulente DA, Kominek J, Zhou X, Steenwyk JL, Buh KV, et al. Tempo and Mode of Genome Evolution in the Budding Yeast Subphylum. Cell. 2018; 175(6):1533–45 e20. Epub 2018/11/13. https://doi.org/10.1016/j.cell.2018.10.023 PMID: 30415838; PubMed Central PMCID: PMC6291210.

83. Bassilana M, Blyth J, Arkowitz RA. Cdc24, the GDP-GTP exchange factor for Cdc42, is required for invasive hyphal growth of Candida albicans. Eukaryot Cell. 2003; 2(1):9–18. Epub 2003/02/13. https://doi.org/10.1128/EC.2.1.9-18.2003 PMID: 12582118; PubMed Central PMCID: PMC141177.

84. Ram AF, Klis FM. Identification of fungal cell wall mutants using susceptibility assays based on Calcofluor white and Congo red. Nat Protoc. 2006; 1(5):2253–6. Epub 2007/04/05. https://doi.org/10.1038/nprot.2006.397 PMID: 17406464.

85. Wilson RB, Davis D, Mitchell AP. Rapid hypothesis testing with Candida albicans through gene disruption with short homology regions. J Bacteriol. 1999; 181(6):1868–74. Epub 1999/03/12. https://doi.org/10.1128/JB.181.6.1868-1874.1999 PMID: 10074081; PubMed Central PMCID: PMC93587.

86. Bijlani S, Thevandavakkam MA, Tsai HJ, Berman J. Autonomously Replicating Linear Plasmids That Facilitate the Analysis of Replication Origin Function in Candida albicans. mSphere. 2019; 4(2). Epub 2019/03/08. https://doi.org/10.1128/mSphere.00103-19 PMID: 30842269; PubMed Central PMCID: PMC6403455.

87. Lai WC, Sun HF, Lin PH, Ho Lin HL, Shieh JC. A new rapid and efficient system with dominant selection developed to inactivate and conditionally express genes in Candida albicans. Curr Genet. 2016; 62(1):213–35. Epub 2015/10/27. https://doi.org/10.1007/s00294-015-0526-6 PMID: 26497136.

88. Schaub Y, Dunkler A, Walther A, Wendland J. New pFA-cassettes for PCR-based gene manipulation in Candida albicans. J Basic Microbiol. 2006; 46(5):416–29. Epub 2006/09/30. https://doi.org/10.1002/jobm.200510133 PMID: 17009297.

89. Gerami-Nejad M, Zacchi LF, McClellan M, Matter K, Berman J. Shuttle vectors for facile gap repair cloning and integration into a neutral locus in Candida albicans. Microbiology (Reading). 2013; 159(Pt 3):565–79. Epub 2013/01/12. https://doi.org/10.1099/mic.0.064097-0 PMID: 23306673; PubMed Central PMCID: PMC3709822.

90. Li L, Zhang C, Konopka JB. A Candida albicans temperature-sensitive cdc12-6 mutant identifies roles for septins in selection of sites of germ tube formation and hyphal morphogenesis. Eukaryot Cell. 2012; 11(10):1210–8. Epub 2012/08/14. https://doi.org/10.1128/EC.00216-12 PMID: 22886998; PubMed Central PMCID: PMC3485918.

91. Puerner C, Kukhaleishvili N, Thomson D, Schaub S, Noblin X, Seminara A, et al. Mechanical force-induced morphology changes in a human fungal pathogen. BMC Biol. 2020; 18(1):122. Epub 2020/09/12. https://doi.org/10.1186/s12915-020-00833-0 PMID: 32912212; PubMed Central PMCID: PMC7488538.

92. Silva PM, Puerner C, Seminara A, Bassilana M, Arkowitz RA. Secretory Vesicle Clustering in Fungal Filamentous Cells Does Not Require Directional Growth. Cell Rep. 2019; 28(8):2231–45 e5. Epub 2019/08/23. https://doi.org/10.1016/j.celrep.2019.07.062 PMID: 31433995.

93. Bassilana M, Hopkins J, Arkowitz RA. Regulation of the Cdc42/Cdc24 GTPase module during Candida albicans hyphal growth. Eukaryot Cell. 2005; 4(3):588–603. Epub 2005/03/10. https://doi.org/10.1128/EC.4.3.588-603.2005 PMID: 15755921; PubMed Central PMCID: PMC1087799.

94. Sanchez AA, Johnston DA, Myers C, Edwards JE Jr., Mitchell AP, Filler SG. Relationship between Candida albicans virulence during experimental hematogenously disseminated infection and endothelial cell damage in vitro. Infect Immun. 2004; 72(1):598–601. Epub 2003/12/23. https://doi.org/10.1128/IAI.72.1.598-601.2004 PMID: 14688143; PubMed Central PMCID: PMC344013.